

University of Alberta

Library Release Form

Name of Author: Jiang Feng

Title of Thesis: Rock Properties Inversion with Kirchhoff AVA Migration/Inversion

Degree: Master of Science

Year this Degree Granted: 2004

Permission is hereby granted to the University of Alberta Library to reproduce single copies of this thesis and to lend or sell such copies for private, scholarly or scientific research purposes only.

The author reserves all other publication and other rights in association with the copyright in the thesis, and except as herein before provided, neither the thesis nor any substantial portion thereof may be printed or otherwise reproduced in any material form whatever without the author's prior written permission.

Jiang Feng
Department of Physics
University of Alberta
Edmonton, AB Canada T6G 2J1

Date: October 20, 2004

Beyond the gate of experience flows the Way,
Which is ever greater and more subtle than the world.

——Lao Tze

University of Alberta

ROCK PROPERTIES INVERSION WITH KIRCHHOFF AVA MIGRATION/INVERSION

by

Jiang Feng

A thesis submitted to the Faculty of Graduate Studies and Research in partial fulfillment of the requirements for the degree of **Master of Science**.

in

Geophysics

Department of Physics

Edmonton, Alberta
Fall 2004

University of Alberta

Faculty of Graduate Studies and Research

The undersigned certify that they have read, and recommend to the Faculty of Graduate Studies and Research for acceptance, a thesis entitled **Rock Properties Inversion with Kirchhoff AVA Migration/Inversion** submitted by Jiang Feng in partial fulfillment of the requirements for the degree of **Master of Science** in *Geophysics*.

Dr. Mauricio. D. Sacchi (Supervisor)

Dr. Moritz H. Heimpel

Dr. Lawrence H. Le

Dr. Martyn Unsworth

Date: _____

To
Yiqian

Abstract

Rock properties inversion for complex structure subsurface is an important issue for today's seismic exploration. Three factors determine the major contribution to the efficiency and accuracy of the inversion: the imaging technique must obey physical principle of wave propagation, proper inverse theory, and suitable noise reduction.

Taking the three factors into account, I propose a strategy to perform rock physical properties inversion based on an amplitude versus angle (AVA) imaging technique, thus called pre-stack depth migration based rock physical parameters inversion. The foundation is Kirchhoff migration and Aki & Richards approximation to Zoeppritz equation, which use the Kirchhoff integral formulation to estimate rock physical parameters directly from pre-stack seismic data. High accuracy is achieved by integrating AVO/AVA and imaging together.

The least squares method is used to minimize a data space misfit and a model space regularization term. The weighted misfit term measures the data reconstruction fidelity. The weighted model space regularization enforces the inverted rock physical parameters consistency along the horizontal plane and sparseness along the vertical direction. Rock physical properties are retrieved by applying the conjugate gradient (CG) method on a ray-based Kirchhoff migration/inversion scheme in the angle domain. The Green's functions of the wave field are calculated using target oriented ray-tracing and stored in memory in advance. Therefore, the algorithm avoids additional calculations at each iteration.

Acknowledgements

I would like to express my gratitude to my supervisor Dr. Mauricio Sacchi for the opportunity to work with a "**True Amplitude**". Both his guidance and propelling help me a great deal during my research.

I extend my thanks to the members of my examining committee for their valuable suggestions and for agreeing to read my thesis.

Thanks to my fellow students at the University of Alberta for precious discussions and suggestions. Especially for my classmate in SAIG and Dr. Ulrich Theune. I would also like to acknowledge the staff of the Physics Department for doing a great job.

Many thanks to all of my friends for their kindness and friendships, for reminding me of "true life" beyond "studying".

Special thanks to my family for proofreading my thesis and lighting my life in darkness.

Contents

1	Introduction	1
1.1	Background	1
1.1.1	True amplitude migration	2
1.1.2	Why a Kirchhoff migration/inversion approach?	3
1.1.3	AVO/AVA	4
1.2	Thesis motivation	6
1.3	Scope of the thesis	7
2	Kirchhoff modeling/adjoint operators for angle dependent reflectivity	9
2.1	Introduction	9
2.2	The basic wave equation	11
2.2.1	The elastic wave equation	11
2.2.2	The acoustic wave equation	13
2.3	Linearizing the scattering problem	13
2.3.1	Solution of the wave equation	14
2.3.2	Kirchhoff approximation	15
2.4	Asymptotic inversion	17
2.5	Modeling operators of linear scattering problem	18
2.5.1	Forward modeling	19
2.5.2	Adjoint modeling	19
2.5.3	Implementation of modeling operators	20

2.6	Summary	23
3	Forward/adjoint operators for rock property inversion	24
3.1	Introduction	24
3.2	A&R approximation to the Zoeppritz equations	25
3.3	Modeling operators for A&R approximation	27
3.3.1	Forward modeling	28
3.3.2	Adjoint modeling	29
3.4	Implementation of modeling operators	29
3.5	Integrating AVA inversion with Kirchhoff migration	30
3.6	Summary	31
4	Inversion of angle gathers and rock properties	32
4.1	Introduction	32
4.2	Discrete inversion theory	33
4.2.1	Seismic discrete inversion problem	33
4.2.2	Constraints	35
4.3	Constrained least-squares migration/inversion	41
4.3.1	Conjugate gradients implementation	42
4.3.2	Forward/adjoint operator for inversion	42
4.4	Implementation of the inversion algorithm	44
4.5	Summary	44
5	Target oriented ray tracing for Green's function	46
5.1	Introduction	46
5.2	Target oriented ray tracing	47
5.2.1	The macro-velocity model	48
5.2.2	The Green's function	49
5.3	Travel times approximation	50
5.3.1	Accuracy of the travel times approximation	51
5.4	Geometrical spreading/amplitude approximation	53

5.4.1	Accuracy of the amplitude approximation	55
5.5	Summary	56
6	Synthetic and field data examples	58
6.1	Introduction	58
6.2	Synthetic data examples	59
6.2.1	Seismic modeling for synthetic data test	59
6.2.2	Inverse algorithm for 2D acoustic synthetic data	60
6.2.3	Simple model with structures	61
6.2.4	Marmousi model	70
6.3	Real data example	79
6.4	Summary	80
7	Conclusions	85
	References	87

List of Tables

6.1	Acquisition geometry for synthetic model	61
6.2	Acquisition geometry for Marmousi model	71
6.3	Acquisition geometry for Gulf of Mexico data set	80

List of Figures

1.1	Amplitude versus angle (AVA)	5
1.2	Work flow for rock properties inversion	7
2.1	A special choice of closed surface \check{S} for the derivation of the Kirchhoff integrals	15
2.2	Coordinates for AVA Kirchhoff migration/inversion	18
2.3	Inversion retrieves better image than migration	21
3.1	Coordinates for reflectivity	27
5.1	Target oriented ray tracing	47
5.2	Sketch of a filter grid	48
5.3	Comparing of analytic result with ray racing. Background is travel-time error(maximum error is less than 0.0039 seconds). The source is located at (5000m, 5000m).The wavefront is contoured in 0.080 seconds increments.	51
5.4	Comparing Snell Law model with ray racing. Background is layer velocity. The source is located at (4900m,4700m).	52
5.5	Relative travelttime errors that are computed with the Snell law model at the surface.	53
5.6	Amplitude in constant velocity media, initial angle is 0° (A), and any angle (B).	54

5.7	Comparing amplitude between analytic method and approximate method using constant velocity model. The source is located at (8000 m, 8000m). The amplitude contour increment is 0.1.	55
5.8	Comparing amplitude between analytic method and approximate method using gradient velocity model ($v = 3000 + 0.4z$). The source is located at (8000 m, 8000m). The amplitude contour increment is 0.1.	56
5.9	Relative amplitude error between analytic method and approximate method using gradient velocity model $v = a + b.z$ [m/s]. The source is located at (8000 m, 8000 m). $a = 3000$ and $b = 0$ (A), 0.1 (B), 1 (C), 10 (D), 100 (E), and 1000 (F). The initial angle is 0° (blue), 15° (green), 30° (red), 45° (yellow), 60° (black), 75° (magenta). Note that the relative error is small (less than 0.5%).	57
6.1	Simple model with structures	61
6.2	Common shot gather of synthetic data	63
6.3	Macro velocity model for synthetic data	64
6.4	Comparison the structure of the inverted image with the true model .	65
6.5	Inverted CIGs and corresponding AVA for synthetic data	66
6.6	Inverted perturbations of velocity and density	68
6.7	Comparing original data with reconstructed data	69
6.8	Data misfit	70
6.9	Marmousi model	73
6.10	Inverted Marmousi image and rock properties	74
6.11	Inverted CIGs and corresponding AVA for Marmousi data	75
6.12	Inverted perturbations of velocity and density for Marmousi model at $x = 3600$ m	76
6.13	Inverted perturbations of velocity and density for Marmousi model at $x = 6425$ m	77
6.14	Comparing Marmousi data with reconstructed data	78
6.15	Near offset section with the study area	81

6.16	The macro velocity model for real data	82
6.17	Inverted perturbations for real data	83
6.18	Common image gather at $CMP = 1069$ for real data	84

Table of Symbols

Symbol	Name or description
α_1, α_2	ray parameter
c_{ijkl}	stiffness tensor
c_p, c_s	P-, S-wave velocity
e_{kl}	strain tensor
f	source function
ρ	density
\vec{n}	normal direction unit
v, v_p, v_s	velocity, P-wave, S-wave velocity
ϕ, ψ	Lamé potential
λ, μ	Lamé constants
λ, μ	tradeoff parameters
s_{ij}	source strain tensor
τ_{ij}	stress tensor
t	time
u_i	particle displacement vector or wave field
u_I, u_S	incident, scattered wave field
ω	angular frequency
θ	reflection angle
δ	discrete version of the delta function, $\delta_{ij} = \begin{cases} 0 & i \neq j \\ 1 & i = j \end{cases}$
\dagger	superscript for pseudoinverse
\mathbf{I}	identity operator
\mathcal{J}	cost function
\mathcal{K}	Kirchhoff operator
\mathcal{L}	integral operator

Symbol	Name or description
AVA	amplitude versus angle
AVO	amplitude variations with offset
A&R	Aki and Richards approximation
CG	conjugate gradient
\mathcal{C}	source wavelet operator
CIGs	common image gathers
CMP	common mid-point
CWP	Center for Wave Phenomena
D	weighting matrix
\mathbf{d}	data
F	filter operator
FD	finite difference
\mathbf{G}	matrix operator
GB	Gigabytes – 10^9 bytes
GRT	generalized Radon transform
\mathbf{m}	model
\mathbf{n}	additive noise
\mathbf{p}	slowness vector
PSDM	pre-stack depth migration
R	angle dependant reflectivity
\mathbf{s}, \mathbf{r}	source, and receiver
T	superscript for transpose
W	wavelet
Z	A&R approximate operator to Zoeppritz equation

Chapter 1

Introduction

1.1 Background

Seismic migration is the most effective geophysical method for imaging the complex structure of the Earth. Today, the goal of the migration extends from imaging subsurface structures to recovering elastic properties (Beydoun and Mendes, 1989). As rock physical parameters are not related linearly to the seismic reflection data (Lumley and Beydoun, 1997), the inversion for elastic constants should be performed in two steps:

1. Pre-stack depth migration/inversion (PSDM), where the seismic data are transformed to common image gathers (CIGs) by migration or inversion. This step requires a migration algorithm for complex media that preserves amplitudes.
2. Amplitude versus angle (AVA) or amplitude variation with offset (AVO) analysis by using approximations to the Zoeppritz equations (Aki and Richards, 1980; Shuey, 1985; Fatti et al., 1994), the CIGs are transformed to perturbations of the elastic parameters (Beretta et al., 2002; Li et al., 2003).

Both AVA analysis and PSDM technologies have made great progress in the last two decades. However, pre-stack migration and AVA/AVO analysis technologies are developed by people with different goals in mind, and, consequently, AVO-based analysis of rock properties are rarely incorporated into sophisticated migration procedures (Xu, 2003). The pre-stack migration has great advantages at the time of

imaging complex geological structures over other seismic processing schemes. Therefore, integrating AVO and imaging together should lead to a new class of algorithms capable of imaging the Earth's interior and retrieving the physical properties (Downton and Lines, 2003).

1.1.1 True amplitude migration

As one part of the inversion, true amplitude migration plays a very important role in our algorithm. This is because it is "capable of undoing distortions of wave propagation between the sources and the receivers and thus producing angle dependent reflection coefficients at analysis points in a lossless, isotropic, elastic earth" (Gray, 1997). Migration has been implemented since the 1920's as a graphical method, but imaging was the primary goal of the migration at that time, AVO/AVA preserved CIGs was not considered during the first 60 years of the migration developments. Fortunately, many geophysicists have been investigating amplitude preserving migration since 1980. Today, several migration methods are available. Gray (1997) separated them into three categories:

1. The Delft migration/inversion approach developed by Berkhout (1985) and his colleagues (de Bruin et al., 1990; de Bruin, 1992; Berkhout and Wapenaar, 1993) at Delft University of Technology. Their method is based on an algorithm that extrapolates wave fields up and down to the reflection point.
2. The CWP migration/inversion approach developed by Bleistein and his colleagues (1987; 2001; 2002a; 2002b) at the Center for Wave Phenomena at the Colorado School of Mines. Such method is based on the theory which expresses the scattering wave field as an integral of angle dependent reflectivity.
3. The least squares migration/inversion approach started by Tarantola (1984) and developed by others internationally (LeBras and Clayton, 1988; Beydoun and Mendes, 1989; Lumley and Beydoun, 1997; Xu et al., 2001; Kuehl and Sacchi, 2003). This method minimizes a misfit for all the data of entire survey.

Although there are some other methods, all of them can be categorized into one or a combination of the aforementioned methods. Further, even the three methods differ in the derivation, implementation, and applicability, there are some fundamental similarities among them. For example, all methods are based on wave propagation theory and ignore the losses caused by the conversion of energy from one elastic model to another, anisotropy, attenuation, and fine layering.

The method described in this thesis is mainly based on the work developed by Bleistein (1987; 2001; 2002a; 2002b) and Xu et al. (2001) on Kirchhoff migration/inversion. In particular, we implement our algorithm as a regularized least squares migration problem where we estimate elastic parameter perturbations directly from the pre-stack data volume. In one word, our method is the Kirchhoff least squares migration/inversion approach.

1.1.2 Why a Kirchhoff migration/inversion approach?

Precise imaging the Earth interior and determination of material properties are a chief goal for exploration practitioners. Many migration methods have been developed. However, most migration methods are based on two basic wave solutions. One class of methods is based on the direct solution of the wave equation, such as numerical finite difference. Another class of methods is based on the asymptotic linear solution of the wave equation, such as the Kirchhoff imaging method. Comparing to the black box operator—numerical finite difference method, Kirchhoff approximation method allows us to do a theoretical analysis of the inversion problem. Furthermore, Kirchhoff migration is more efficient and flexible than wave equation migration. Therefore, I mainly concentrate on the Kirchhoff + ray tracing asymptotic imaging method.

The fundamental work of asymptotic imaging was done by Beylkin (1985; 1990). Bleistein (1987; 2001) extended his work to work with reflection data. Burridge et al. (1998) developed the theory for heterogeneous, anisotropic elastic medium. In order to overcome artifacts appearing in pre-stack common image gathers (CIGs)

generated by common offset (or common shot) depth migration for complex media, Xu, et al. (2001), based on the previous work by de Hoop et al. (1994), proved that computing CIGs in refracting/reflecting angle domain satisfies the imaging condition¹ in most cases. Bleistein et al. (2002b) proposed a method for common angle migration/inversion. His work forms the foundation of our algorithm.

Asymptotic inverse to the generalized Radon transform (GRT) (Beylkin, 1985; Bleistein, 1987) is also called migration (Youzwishen, 2001) or direct inversion, which directly recovers an image of the Earth. There is another kind of inverse method called discrete inversion, which minimizes the difference between observed data and synthetic data. Jin et al. (1992) combined the two methods to form what is called the migration/inversion scheme. Such method can find the best solution when complete information is unavailable. Thus, it partially corrects the problem caused by the limited recording aperture, which is a common problem among most imaging methods.

Since the unit of size for seismic data is GB (10^9 bytes), solutions that involve the inversion of operators that after discretization lead to large matrices are not feasible. One way to avoid this problem is by using the Conjugate Gradients (CG) methods. Another chief advantage of CG for solving large system of equations is that the explicit matrix forms are not needed. Thus, we use Kirchhoff least squares migration/inversion approach.

1.1.3 AVO/AVA

Reflection of plane waves at a plane boundary constitutes the framework for our analysis. It builds a bridge between the rock physical properties at a reflection point and the amplitudes of scattered waves. Zoeppritz (1919) was among the first to investigate and discover a set of analytic relationships for reflecting waves at interfaces. Those equations, named Zoeppritz equations, are the foundation of modern AVO/AVA analysis. Since the Zoeppritz equations are very complex, the

¹Imaging condition means that all the locally coherent events in the data are focused at a single position after migration/inversion.

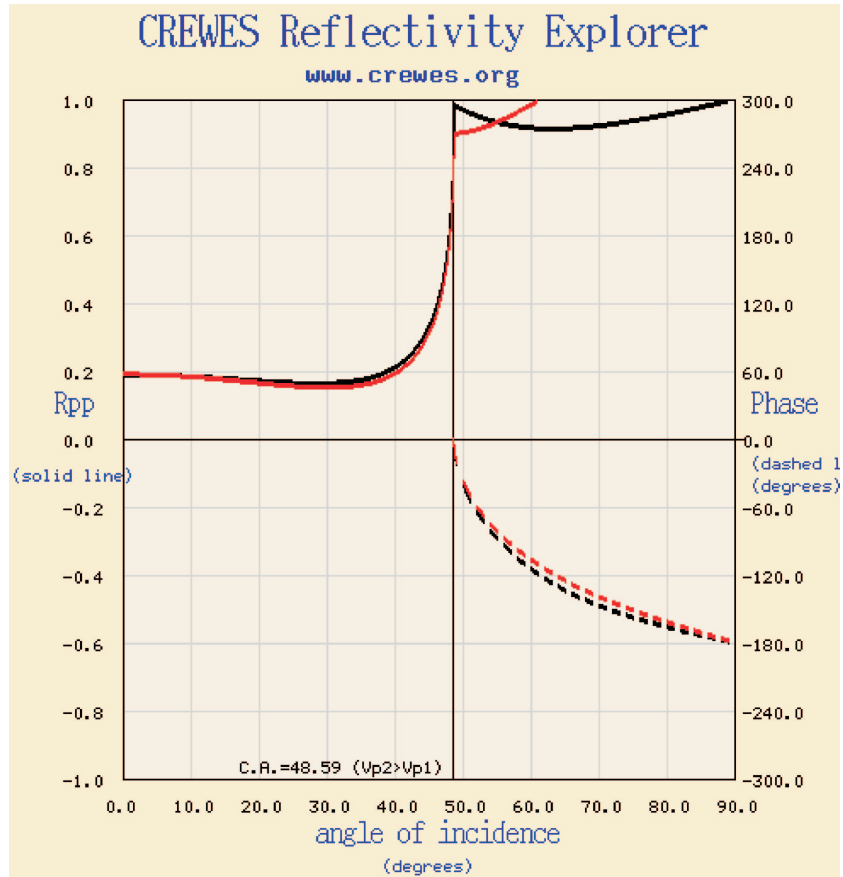


Figure 1.1: Amplitude (reflectivity) versus angle (AVA), the red line represents the A&R approximation, and the black line refers to exact result.

inverse problems for estimating rock properties from angle dependent reflectivity are mainly based on approximate analytic expression for reflection coefficients (Aki and Richards, 1980; Shuey, 1985; Fatti et al., 1994). Figure 1.1 shows the comparison of the true AVA and the one obtained from A&R approximation. A free software application of CREWES reflectivity explorer (from University of Calgary) was used to obtain the result.

There are two important applications for reflection coefficients studies. First is direct inversion for rock properties (Beydoun and Mendes, 1989; Lumley and Beydoun, 1997; Downton and Lines, 2002; Downton and Lines, 2003; Feng and Sacchi, 2004b). Such method inverts the perturbation of elastic parameters (i.e.,

density, P-wave, and S-wave velocities) from CIGs using linearized approximation to Zoeppritz equations. As the variation of P-wave amplitude coefficients with reflection angle is influenced by density, P-wave, and S-wave velocities on both sides of a reflecting boundary, and the reflection angles of P-wave are easily calculated. Usually, P-wave amplitude coefficients are used for the elastic parameters inversion. The second is the analysis of amplitude variations with offset (AVO) or amplitude versus angle (AVA). AVO/AVA anomalies, which indicate areas of changes in rock physical properties, can thus be used as oil/gas indicator for seismic exploration (Li et al., 2003; Kuehl and Sacchi, 2003). The most famous example is "bright spots" which resulted in the discovery of many oil/gas fields.

In this thesis, I propose an algorithm which directly inverts elastic parameter perturbations from the pre-stack data, then, CIGs are generated by mapping the rock parameter vector to the common image gather panel using a linearized approximation to Zoeppritz equations. This is an important difference with respect to earlier strategies proposed by Kuehl and Sacchi (2003) where lateral smoothness was directly imposed on the common image gather rather than on the vector of rock parameters. Figure 1.2 shows a overview of for our lab work flow. The forward operators are derived using the Kirchhoff approximation to linearize the wave equation. The least squares inverse theory is applied to obtain a better solution, and then the result is visualized to decide if the inverted results are reasonable.

1.2 Thesis motivation

Nowadays, the main role of migration extends from imaging subsurface structure to providing detailed information about subsurface rock properties. However, the rock properties inversion is often done in two steps. The processors transform the seismic data to the image of the reservoir. Then, reservoir geologists interpret the image in terms of structure, stratigraphy, and rock properties. There is relative less work being done to directly relate the pre-stack seismic data to the rock properties (Lumley and Beydoun, 1997). A reasonable goal, therefore, is to combine those two

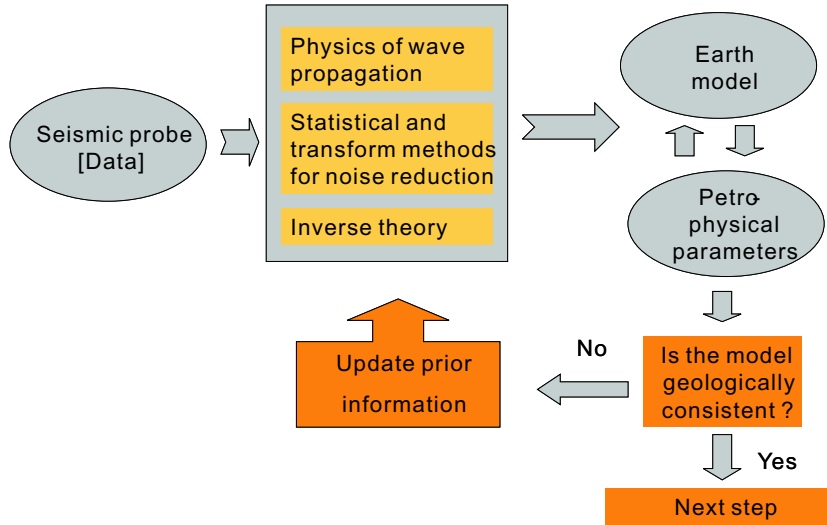


Figure 1.2: Work flow of our lab for rock properties inversion.

steps together by incorporating AVO/AVA-based analysis of rock properties into sophisticated migration procedures. Such inversion for rock properties is not new. Some geophysicists have worked on this problem (Tarantola, 1986; Beydoun and Mendes, 1989; Lumley and Beydoun, 1997; Downton and Lines, 2003).

1.3 Scope of the thesis

In this thesis, I proposed a method for AVA migration/inversion. The rock physical properties are inverted directly from pre-stack seismic data by applying the conjugate gradient (CG) method on a ray-based Kirchhoff migration/inversion scheme in the angle domain. l_2 and l_1 norms are used as regularization terms to improve the smoothness along horizontal plane, as well as the vertical resolution. The implementation of this method shows a successful delineation of subsurface structures and an accurate recovering of local changes in rock physical properties for 2D synthetic and real seismic data.

This thesis proceeds as follows. In Chapter 1, I discuss the background of AVO/AVA migration/inversion. In Chapter 2, I review the theory of linearizing the scattering problem with Kirchhoff approximation. On the basis of the theory,

I define the forward operator and the adjoint operator which are used by the CG inversion. Another important theory, on which the AVO/AVA analysis is based, is summarized in Chapter 3. The forward operator and the adjoint operator are presented as well. Since the first operator's output is the second operator's input, those two operators are integrated together to form a new forward and adjoint operator couple. As mentioned before, the inverse procedure is done in the framework of the least squares technique. To improve robustness of the algorithm, a weighted regularization term is applied. All the details about the least squares inversion are described in Chapter 4. Since the efficiency of the Green's function's calculation significantly affects the cost of the true amplitude migration, the proposed algorithm for the Green's function computation is presented in Chapter 5. In Chapter 6, the least squares AVA migration for rock properties inversion is applied to synthetic and real data. In Chapter 7, the conclusions of the thesis are discussed. Further research for improvements is also discussed.

Chapter 2

Kirchhoff modeling/adjoint operators for angle dependent reflectivity

2.1 Introduction

In exploration seismology, wave fields are intentionally created to image the interior of the earth. The artificial seismic waves are generated and their reflections from impedance difference within the earth are recorded. In order to invert those recorded data precisely for subsurface structure and elastic physical parameters, the inversion algorithm, which attempts to undo the wave propagation effects, must obey the wave propagation theory (or wave equation).

Due to the difference of deriving the solution of the wave equation, Wave propagation process in complex media is described by two main types (Hertweck, 2000).

1. finite difference, based on direct solution of wave equation (Alford et al., 1974; Lines et al., 1999).
2. approximate high frequency asymptotic methods (e.g., Born or Kirchhoff method), based on the Green's theorem (Beydoun and Mendes, 1989; Duquet et al., 2000).

Since Kirchhoff methods are conceptually simple, versatile, and more efficient (Gray et al., 2001), our research focuses on the second method, such as ray-based

Kirchhoff theory. Like any inverse problem, the linearized forward or modeling theory is the first step.

Seismic forward modeling describes the forward process, which generates synthetic data from a known earth model (Gray et al., 2001). In seismic exploration, all math-physical operators are idealized by ignoring some features of the true nature of the phenomena. More or less, the idealization will bring errors into the result. Without a doubt, a problematic forward operator will lead to a wrong inverse operator. However, if the main physical characters are honored, the inverted results are still successfully used for geophysical exploration (Kuehl, 2002; Bleistein et al., 2001; Gray, 1997).

Using a high-frequency approximation,¹ the Kirchhoff forward operator represents the forward problem with a Kirchhoff integral. This linear scattering integral can be directly inverted using generalized Radon theory and pseudo-differential operator/Fourier integral operator theory (Bleistein, 1987). However, the main disadvantage of the direct inversion is that the result does not fit the data.

In order to overcome this shortcoming, a discrete inversion method is presented in my study. This method approaches the true earth image iteratively doing forward and adjoint processing. Such technique is called migration/inversion scheme (Duquet et al., 2000; Youzwishen, 2001).

In general, the common image gathers (CIGs) are obtained after migration (or inversion). In complex media, CIGs can be computed using algorithms designed to obtain angle dependent reflectivity (Xu et al., 2001).

In this chapter, basic formulas of the wave propagation theory are presented. Then, I review the theory of the linearizing scattering problem with the Kirchhoff integral which leads to Bleistein's general approach to common angle migration/inversion method (Bleistein and Gray, 2002b). On the basis of the migra-

¹High-frequency refers to the frequency content of the waves "high" in relative sense. It means that the length of target in the medium is many times larger than the length of wavelet of the seismic wave (or the velocity of the medium should vary very slowly). Although our inverse theory is based on high-frequency approximation, the method would not totally fail if the high-frequency condition does not exactly satisfied (Bleistein et al., 2001). Therefore, such asymptotic methods can also be used for complex structure.

tion/inversion theory, I define a forward operator and an adjoint operator that are implemented numerically in Fortran subroutines.

The method described in this chapter is based on the equation that was deduced by Bleistein et al (2002b). The subroutines, representing the forward and the adjoint operators, were originally developed by Dr. Sacchi and improved by the author.

2.2 The basic wave equation

Algorithms derived from the wave equation play an important role in the seismic industry. The wave equation describes the medium properties as a function of the physical parameters. Here I review the basic wave equation with the Lagrangian description².

2.2.1 The elastic wave equation

Consider an elastic body. The linearized equation of motion (generalized Newton's Second Law) is described as

$$\tau_{ij,j} - \rho u_{i,tt} = -f_i, \quad (2.2.1)$$

where $i, j = 1, 2, 3$ stand for x, y, z respectively; τ represents the stress tensor; f represents the source function; ρ is the density of the solid ; u_i refers to the particle displacement vector.

In addition, τ_{ij} and u_i can also be described by linearized stress-strain relation (generalized Hooke's Law)

$$\tau_{ij} - c_{ijkl}e_{kl} = -s_{ij}, \quad (2.2.2)$$

where c_{ijkl} represents the stiffness tensor; e_{kl} represents the strain tensor; s_{ij} refers to the source strain tensor.

²Lagrangian description emphasizes the study of a particle that is specified by its original position at some reference time (Aki and Richards, 1980).

In the isotropic case we can reduce the number of independent stiffness coefficients in equation (2.2.2) to two by

$$c_{ijkl} = \lambda \delta_{ij} \delta_{kl} + \mu (\delta_{ik} \delta_{jl} + \delta_{il} \delta_{jk}),$$

with λ and μ being known as the Lamé constants.

Substituting the strain-displacement relations $e_{ij} = \frac{1}{2}(u_{i,j} + u_{j,i})$ to stress-strain relation equation (2.2.2), then substituting result to equation of motion (2.2.1), finally, we obtain stress-displacement relation

$$(c_{ijkl} u_{k,l})_{,j} - \rho u_{i,tt} = -f_i. \quad (2.2.3)$$

In case of homogeneity, above equation can be simplified to

$$(\lambda + 2\mu) \nabla(\nabla \cdot \vec{u}) + \mu \nabla \times \vec{u} - \rho \frac{\partial^2 \vec{u}}{\partial t^2} = -\vec{f}, \quad (2.2.4)$$

where

$$\nabla = \vec{i} \frac{\partial}{\partial x} + \vec{j} \frac{\partial}{\partial y} + \vec{k} \frac{\partial}{\partial z}.$$

Now defining the Lamé potential ϕ and ψ as

$$\vec{u} = \nabla \phi + \nabla \times \vec{\psi}, \quad (2.2.5)$$

we obtain the wave equation for a homogeneous, isotropic solid

$$\nabla^2 \phi - \frac{1}{c_p^2} \frac{\partial^2 \phi}{\partial t^2} = -f_\phi, \quad (2.2.6)$$

for a compressional wave, where $c_p = \sqrt{\frac{\lambda+2\mu}{\rho}}$, and

$$\nabla^2 \vec{\psi} - \frac{1}{c_s^2} \frac{\partial^2 \vec{\psi}}{\partial t^2} = -\vec{f}_\psi, \quad (2.2.7)$$

for a shear wave, where $c_s = \sqrt{\frac{\mu}{\rho}}$.

2.2.2 The acoustic wave equation

When seismic waves propagate through a fluid medium (such as water or oil) in which $\mu = 0$, the elastic wave equation (2.2.4) reduces to

$$\nabla(\lambda \nabla \cdot \vec{u}) - \rho \frac{\partial^2 \vec{u}}{\partial t^2} = -\vec{f}. \quad (2.2.8)$$

Instead of using the displacement vector $\vec{u}(\vec{x}, t)$, it is more common to use the pressure p

$$p(\vec{x}, t) = -\lambda \nabla \cdot \vec{u}(\vec{x}, t). \quad (2.2.9)$$

First dividing both sides of equation (2.2.8) with ρ , then taking divergence of both sides, next, substituting equation (2.2.9) to the result, finally, one obtains

$$\nabla \cdot \left(\frac{1}{\rho} \nabla p \right) - \frac{1}{\lambda} \frac{\partial^2 p}{\partial t^2} = -\tilde{f}, \quad (2.2.10)$$

where $\tilde{f} = \nabla \cdot \left(\frac{1}{\rho} \vec{f} \right)$. If the medium with constant density ρ , above equation can be simplified as

$$\nabla^2 p - \frac{1}{c^2} \frac{\partial^2 p}{\partial t^2} = -\tilde{f}, \quad (2.2.11)$$

where $c = \sqrt{\frac{\lambda}{\rho}}$ is the acoustic wave velocity.

2.3 Linearizing the scattering problem

As a well-established theory, the linear inverse theory makes geophysical inverse problems tractable (Claerbout, 1992). So the scattering wave fields are usually simplified linearly to the perturbation of the physical parameters by ignoring nonlinear parts³ based on high frequency assumption.

³Generally, the linear events correspond to the primary reflections which are caused by perturbation of underground and the nonlinear events correspond to the multiple reflections of those subsurfaces. Therefore, linear inverse theory is valid for de-multiple data.

2.3.1 Solution of the wave equation

Assuming an infinite space with two layers, a point source \mathbf{s} is generated in the upper layer, then in the upper layer, the wave field satisfies

$$\nabla^2 u(\mathbf{x}, \mathbf{s}, \omega) + \frac{\omega^2}{c^2(\mathbf{x})} u(\mathbf{x}, \mathbf{s}, \omega) = -\delta(\mathbf{x} - \mathbf{s}). \quad (2.3.1)$$

where $c(\mathbf{x})$ is the wave speed, \mathbf{x} is the arbitrary position, ω is the angular frequency, $u(\mathbf{x}, \mathbf{s}, \omega)$ is the total wave field which is composed from the incident wave field $u_I(\mathbf{x}, \mathbf{s}, \omega)$ generated by the point source and the scattered wavefield $u_S(\mathbf{x}, \mathbf{s}, \omega)$ generated by the interface between two layers, then the equation (2.3.1) can be written as

$$\nabla^2 u_S(\mathbf{x}, \mathbf{s}, \omega) + \frac{\omega^2}{c^2(\mathbf{x})} u_S(\mathbf{x}, \mathbf{s}, \omega) = -[\nabla^2 u_I(\mathbf{x}, \mathbf{s}, \omega) + \frac{\omega^2}{c^2(\mathbf{x})} u_I(\mathbf{x}, \mathbf{s}, \omega)] - \delta(\mathbf{x} - \mathbf{s}), \quad (2.3.2)$$

and the incident wave field $u_I(\mathbf{x}, \mathbf{s}, \omega)$ satisfies the Green's function under the high frequency assumption

$$\nabla^2 u_I(\mathbf{x}, \mathbf{s}, \omega) + \frac{\omega^2}{c^2(\mathbf{x})} u_I(\mathbf{x}, \mathbf{s}, \omega) = -\delta(\mathbf{x} - \mathbf{s}). \quad (2.3.3)$$

Substituting this equation to equation (2.3.2), one obtains

$$\nabla^2 u_S(\mathbf{x}, \mathbf{s}, \omega) + \frac{\omega^2}{c^2(\mathbf{x})} u_S(\mathbf{x}, \mathbf{s}, \omega) = 0. \quad (2.3.4)$$

In order to solve above equation, the Green's theorem, "which allows us to represent a wavefield on either of a surface of infinite extent in terms of the wavefield and its normal derivative on the surface" (Bleistein et al., 2001), is used. We define another Green's function $G(\mathbf{r}, \mathbf{x}, \omega)$

$$\nabla^2 G(\mathbf{r}, \mathbf{x}, \omega) + \frac{\omega^2}{c^2(\mathbf{x})} G(\mathbf{r}, \mathbf{x}, \omega) = -\delta(\mathbf{r} - \mathbf{x}), \quad (2.3.5)$$

with \mathbf{r} being the receiver position, and \mathbf{x} arbitrary point in the upper layer. Apply the Green's theorem to equation (2.3.4) and (2.3.5) in the upper layer. After some manipulations we obtain

$$u_S(\mathbf{r}, \mathbf{s}, \omega) = \oint_{\check{S}} \left[G(\mathbf{x}, \mathbf{r}, \omega) \nabla u_S(\mathbf{x}, \mathbf{s}, \omega) - u_S(\mathbf{x}, \mathbf{s}, \omega) \nabla G(\mathbf{x}, \mathbf{r}, \omega) \right] d\check{S}, \quad (2.3.6)$$

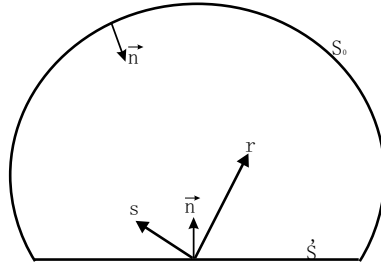


Figure 2.1: A special choice of closed surface \check{S} ($\acute{S} + S_0$) for the derivation of the Kirchhoff integrals. s, r are source, receiver respectively.

where \check{S} is the surface enclosing entire upper layer volume

$$\check{S} = \acute{S} + S_0,$$

where \acute{S} and S_0 are the surfaces of the plane and the half sphere showed in Figure 2.1.

In the physical experiment, energy of any impulse signal will become zero at an infinite boundary, the above equation becomes

$$u_S(\mathbf{r}, \mathbf{s}, \omega) = - \int_{\acute{S}} \left[G(\mathbf{x}, \mathbf{r}, \omega) \frac{\partial u_S(\mathbf{x}, \mathbf{s}, \omega)}{\partial n} - u_S(\mathbf{x}, \mathbf{s}, \omega) \frac{G(\mathbf{x}, \mathbf{r}, \omega)}{\partial n} \right] d\acute{S}, \quad (2.3.7)$$

\vec{n} represents normal direction unit (see Figure 2.1). Because the normal direction is pointed outward from the domain of integration in the Green's theorem, here I define \mathbf{n} upward pointing normal to the interface \acute{S} , so I add minus sign in front of the integral. As it is written, this expression is a non-linear equation, the scattered wavefield is a function of itself. Therefore the Kirchhoff approximation is used to linearize scattered wavefield expression.

2.3.2 Kirchhoff approximation

The Kirchhoff approximation is a method which uses the Kirchhoff integral to approximate solution of scattered wave from an infinite interface. This approximation assumes the relationship between the leading-order incident and upward-scattered wave as

$$u_S = R(\theta)u_I, \quad \frac{\partial u_S}{\partial n} = -R(\theta)\frac{\partial u_I}{\partial n}, \quad \text{on } \acute{S}, \quad (2.3.8)$$

2.3. LINEARIZING THE SCATTERING PROBLEM

where $R(\theta)$ is the angle dependent reflectivity; θ is the specular angle of reflection. Now, I substitute equation (2.3.8) to equation (2.3.7) and after some manipulations, the linearized scattering problem is written as

$$u_S(\mathbf{r}, \mathbf{s}, \omega) = \int_{\acute{S}} R(\mathbf{x}, \theta) \frac{\partial [G(\mathbf{x}, \mathbf{s}, \omega)G(\mathbf{r}, \mathbf{x}, \omega)]}{\partial n} d\acute{S}. \quad (2.3.9)$$

For an arbitrary background velocity field, the Green's functions can be expressed as

$$G(\mathbf{x}, \mathbf{y}, \omega) = e^{i\omega\tau(\mathbf{x}, \mathbf{y})} A(\mathbf{x}, \mathbf{y}),$$

where $\tau(\mathbf{x}, \mathbf{y})$ is the travelttime and defined by the Eikonal equation

$$\frac{1}{c^2(\mathbf{x})} - (\nabla\tau(\mathbf{x}, \mathbf{y}))^2 = 0, \quad (2.3.10)$$

and $A(\mathbf{x}, \mathbf{y})$ is amplitude (geometrical spreading factor) which obeys the transport equation

$$2\nabla\tau(\mathbf{x}, \mathbf{y}) \cdot \nabla A(\mathbf{x}, \mathbf{y}) + A(\mathbf{x}, \mathbf{y}) \nabla^2\tau(\mathbf{x}, \mathbf{y}) = 0. \quad (2.3.11)$$

Then, the scattering problem can be expressed as

$$u_S(\mathbf{r}, \mathbf{s}, \omega) = i\omega \int_{\acute{S}} R(\mathbf{x}, \theta) A(\mathbf{r}, \mathbf{x}, \mathbf{s}) \cdot [\vec{n} \cdot \nabla\tau(\mathbf{r}, \mathbf{x}, \mathbf{s})] \cdot e^{i\omega\tau(\mathbf{r}, \mathbf{x}, \mathbf{s})} d\acute{S}, \quad (2.3.12)$$

where

$$\begin{aligned} A(\mathbf{r}, \mathbf{x}, \mathbf{s}) &= A(\mathbf{r}, \mathbf{x})A(\mathbf{x}, \mathbf{s}) \\ \tau(\mathbf{r}, \mathbf{x}, \mathbf{s}) &= \tau(\mathbf{r}, \mathbf{x}) + \tau(\mathbf{x}, \mathbf{s}), \\ \vec{n} \cdot \nabla\tau(\mathbf{r}, \mathbf{x}, \mathbf{s}) &= -|\nabla\tau(\mathbf{r}, \mathbf{x}, \mathbf{s})| = -\left| \frac{2 \cos \theta}{c(\mathbf{x})} \vec{\nu} \right|, \end{aligned}$$

where $\vec{\nu}$ is the unit vector of the travel time gradients, or the migration dip direction (Bleistein and Gray, 2002b). We finally obtain the linear scattering problem equation⁴

$$u_S(\mathbf{r}, \mathbf{s}, \omega) = S(\omega) \int_{\acute{S}} R(\mathbf{x}, \theta) A(\mathbf{r}, \mathbf{x}, \mathbf{s}) \left| \frac{2 \cos \theta}{c(\mathbf{x})} \right| e^{i\omega\tau(\mathbf{r}, \mathbf{x}, \mathbf{s})} d\acute{S}, \quad (2.3.13)$$

⁴KMAH index K , which account for phase shifts in the Green's functions due to caustics in their ray fields (for details see (Bleistein and Gray, 2002b)), is ignored in this equation for calculation efficiency in our algorithm.

where $S(\omega)$ is the signature defined by

$$S(\omega) = \begin{cases} -i\omega W(\omega) & \text{for 3D} \\ |\omega|W(\omega) & \text{for 2D} \\ \sqrt{|\omega|}\sqrt{\frac{\sigma_s\sigma_r}{\sigma_s+\sigma_r}}e^{3i\pi\text{sgn}(\omega)/4}W(\omega) & \text{for 2.5D} \end{cases}$$

where $W(\omega)$ represents wavelet, σ_s and σ_r are the parameters, which describe out-of-plane behavior with the units of Length²/Time, defined by

$$\frac{d\mathbf{x}}{d\sigma_i} = \mathbf{p}_i \quad i = s, r \quad (2.3.14)$$

with \mathbf{p} being slowness vector.

2.4 Asymptotic inversion

In geophysical exploration, inversion is more complex than other processing, i.e. imaging an earth model from the data. Generally, inversion with perfect data will give a perfect result (Claerbout, 1992). Unfortunately seismic data are incomplete and inaccurate, which make inversion a difficult task. Even more, a general expression of this inversion does not exist. Therefore, approximated expressions are derived with the generalized Radon theory and pseudo-differential operator/Fourier integral operator theory (Beylkin, 1985; Bleistein, 1987). Since common angle migration can obtain an improved, artifact free image, Bleistein and Gray (2002b) proposed an algorithm for common-opening-angle migration (or inversion),

$$\begin{aligned} \hat{R}(\mathbf{x}, \theta, \phi) = & \frac{1}{8\pi^3} \left[\frac{2 \cos \theta}{c(\mathbf{x})} \right]^2 \iint S(\omega) \frac{u_S(\mathbf{r}, \mathbf{s}, \omega)}{A(\mathbf{r}, \mathbf{x}, \mathbf{s})} e^{-i\omega\tau(\mathbf{r}, \mathbf{x}, \mathbf{s})} \left| \vec{\nu} \cdot \frac{\partial \vec{\nu}}{\partial \alpha_1} \times \frac{\partial \vec{\nu}}{\partial \alpha_2} \right| \\ & \cdot \delta(\theta' - \theta) \delta(\phi' - \phi) \left| \frac{\partial(\alpha_1, \alpha_2, \theta', \phi')}{\partial(s_1, s_2, r_1, r_2)} \right| d\omega ds_1 ds_2 dr_1 dr_2, \quad (2.4.1) \end{aligned}$$

where $\hat{R}(\mathbf{x}, \theta, \phi)$ is recovered angle dependent reflectivity, \mathbf{s}, \mathbf{r} are sources and receivers defined by surface coordinates (s_1, s_2, r_1, r_2) , θ refers to the reflection angle (Figure 2.2), ϕ refers to the azimuth, α_1, α_2 refer to any parameter that defines rays.

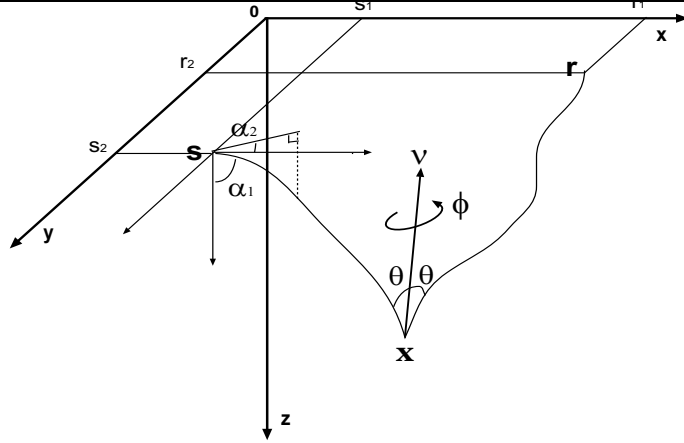


Figure 2.2: Coordinates for AVA Kirchhoff migration/inversion. All variables are referenced to the output point \mathbf{x} . In the neighborhood of \mathbf{x} , the dip \vec{v} , the unit vector in the direction of the ray from the source \mathbf{s} to the output point \mathbf{x} and the unit vector in the direction of the ray from the output point \mathbf{x} to the receiver \mathbf{r} are in the same plane. Those two unit vectors spin around \vec{v} as ϕ varies.

Unfortunately, the reconstructed data, which use the forward operator on inverted model, do not fit the data. Therefore, an iterative constraint method is used to obtain a solution that honors the data.

2.5 Modeling operators of linear scattering problem

Unlike direct inversion (i.e., asymptotic inversion), the discrete inversion technique approximates the inverse by minimizing the difference between the observed data and the synthetic data calculated from the predicted earth model. Thus, the process computing synthetic data from model space to data space, and its inverse process, in some sense, back projecting from data space to model space are needed. These processes are called forward and backward/adjoint (or migration) modeling respectively (Claerbout, 1992; Gray et al., 2001).

2.5.1 Forward modeling

Forward modeling, also called modeling, can be realized by using equation (2.3.13) with a known earth model:

$$u_S(\mathbf{r}, \mathbf{s}, \omega) = S(\omega) \int_V R(\mathbf{x}, \theta) A(\mathbf{r}, \mathbf{x}, \mathbf{s}) \left| \frac{2 \cos \theta}{c(\mathbf{x})} \right| e^{i\omega\tau(\mathbf{r}, \mathbf{x}, \mathbf{s})} W(\omega) d^3\mathbf{x}, \quad (2.5.1)$$

where $R(\mathbf{x}, \theta)$ is the model, $W(\omega)$ represents the source wavelet in frequency domain, and V is the volume of the model one would like to recover.

The last equation can be expressed as a linear Kirchhoff operator, denoted \mathcal{K} , which has two distinct parts: an integral operator \mathcal{L} , and a source wavelet operator \mathcal{C} (or convolution operator in time domain)

$$\begin{aligned} d(\mathbf{r}, \mathbf{s}, \omega) &= \mathcal{K}R(\mathbf{x}, \theta) \\ &= \mathcal{C}\mathcal{L}R(\mathbf{x}, \theta). \end{aligned} \quad (2.5.2)$$

In this equation, $R(\mathbf{x}, \theta)$ is the angle dependent reflectivity, and $d(\mathbf{r}, \mathbf{s}, \omega)$ represents the data. The integral operator is expressed as

$$(\mathcal{L}R)(\mathbf{r}, \mathbf{s}, \omega) = \int R(\mathbf{x}, \theta) A(\mathbf{r}, \mathbf{x}, \mathbf{s}) \left| \frac{2 \cos \theta}{c(\mathbf{x})} \right| e^{i\omega\tau(\mathbf{r}, \mathbf{x}, \mathbf{s})} d^3\mathbf{x}. \quad (2.5.3)$$

The operator \mathcal{C} is given by

$$(\mathcal{C}r)(\omega) = S(\omega)W(\omega)r(\omega), \quad (2.5.4)$$

where $r(\omega)$ is a dummy variable to which the operator is applied, and $S(\omega)$ is defined in equation (2.3.13) without the wavelet term.

2.5.2 Adjoint modeling

Adjoint modeling, also called migration, is an approximated reverse process for removing the forward modeling effects. In the mathematical sense, *adjoint* means the complex conjugate of the matrix transpose (Claerbout, 1992). Thus, the adjoint operator can be derived from forward operator using this definition

$$\begin{aligned} \hat{R}(\mathbf{x}, \theta) &= (\mathcal{C}\mathcal{L})^T d(\mathbf{r}, \mathbf{s}, \omega) \\ &= \mathcal{L}^T \mathcal{C}^T d(\mathbf{r}, \mathbf{s}, \omega), \end{aligned} \quad (2.5.5)$$

where $\hat{R}(\mathbf{x}, \theta)$ is recovered angle dependent reflectivity, and $d(\mathbf{r}, \mathbf{s}, \omega)$ are the data, T means transpose.

The above equation shows that the adjoint operator has two parts corresponding to the forward operator: first undoing the multiply with the conjugate-transpose multiply, and then reversing the summation over the traveltime isochron. To be exact, they can be written as

$$\begin{aligned} d'(\mathbf{r}, \mathbf{s}, \omega) &= (\mathcal{C}^T d)(\mathbf{r}, \mathbf{s}, \omega) \\ &= S(\omega)d(\mathbf{r}, \mathbf{s}, \omega)W^*(\omega), \end{aligned} \tag{2.5.6}$$

$$\begin{aligned} \hat{R}(\mathbf{x}, \theta) &= (\mathcal{L}^T d')(\mathbf{x}, \theta) \\ &= \int A(\mathbf{r}, \mathbf{x}, \mathbf{s})e^{-i\omega\tau(\mathbf{r}, \mathbf{x}, \mathbf{s})} \left| \frac{2 \cos \theta}{c(\mathbf{x})} \right| d'(\mathbf{r}, \mathbf{s}, \omega) d\mathbf{r}d\mathbf{s}d\omega. \end{aligned}$$

Where $d'(\mathbf{r}, \mathbf{s}, \omega)$ is a solution obtained by the adjoint, and $W^*(\omega)$ denotes the conjugate of the wavelet, $A(\mathbf{r}, \mathbf{x}, \mathbf{s})e^{-i\omega\tau(\mathbf{r}, \mathbf{x}, \mathbf{s})}$ the conjugate Green's function.

The adjoint operator in equation (2.5.6) images the structure of the subsurface correctly (Bleistein et al., 2001; Vanelle, 2002) as the inverse operator in equation (2.4.1) does. Both of them use the same phase shift factor $e^{-i\omega\tau(\mathbf{r}, \mathbf{x}, \mathbf{s})}$. But the adjoint operator does not recover full information about the reflectivity as the inverse operator does. To avoid instabilities during inversion, which is common in ill-posed inverse problems, the adjoint operator replaces inversion by multiplication. Therefore, the result is a blurred version of the original image (Youzwishen, 2001). In figure 2.3 we portray the result of using the adjoint and inverse operators to image a 1-D earth structure. As showed in the figure, the inverse process retrieves a more accurate description of the subsurface than the adjoint operator.

2.5.3 Implementation of modeling operators

Since seismic data sets are large and complicated, forward and adjoint modeling can not be expressed simply by matrix operations. Therefore, the subroutines are used to perform these two processes. In order to check that the two subroutines are true

2.5. MODELING OPERATORS OF LINEAR SCATTERING PROBLEM

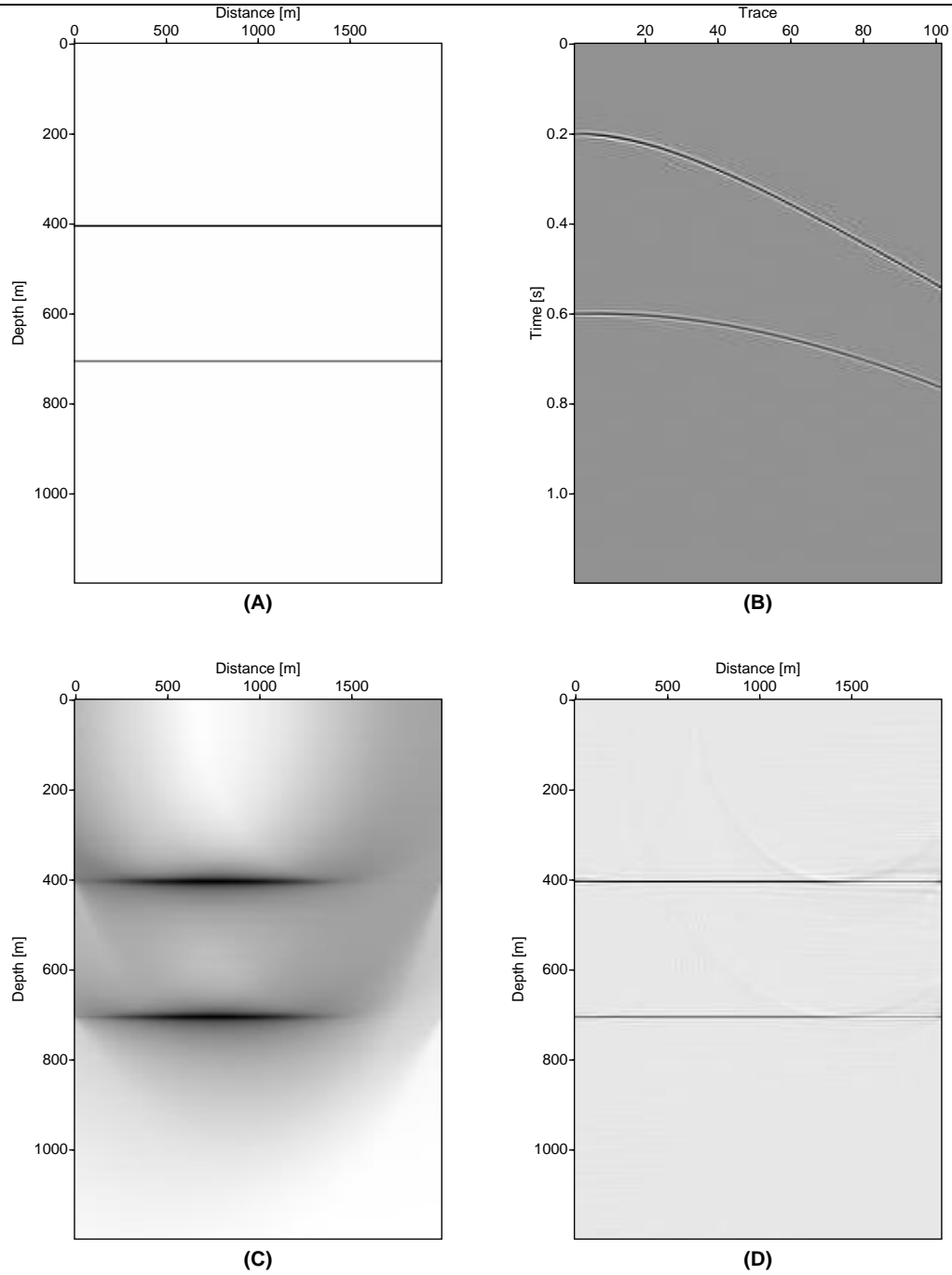


Figure 2.3: (A) The original reflectivity R . (B) Synthetic common shot gather created by the forward operator $d = \mathcal{C}\mathcal{L}R$. (C) The smearred reflectivity recovered by the adjoint operator $\hat{R} = \mathcal{L}^T \mathcal{C}^T d$. (D) The approximated reflectivity retrieved by the iterative inverse technique with forward/adjoint operators.

2.5. MODELING OPERATORS OF LINEAR SCATTERING PROBLEM

adjoints of each other, the dot-product test is used (Claerbout, 1992), which notes

$$\mathbf{y}^T(\mathbf{A}\mathbf{x}) = (\mathbf{A}^T\mathbf{y})^T\mathbf{x}, \quad (2.5.7)$$

where \mathbf{x}, \mathbf{y} are any random vectors or matrices, \mathbf{A} and \mathbf{A}^T represent forward and adjoint processing subroutines respectively.

The pseudo-code for the subroutine is given below. The subroutine named *Kir_for_adj* is for an acoustic earth model. The data are represented in time domain.

```

# Subroutine for Kirchhoff forward/adjoint modeling operators
if  adjoint operator, then
    fast Fourier transform data and multiply signature:  $d_{temp} = \text{fft}(d) * S(\omega)$ 
    conjugate-transpose multiply wavelet with data:  $d_{temp} = \mathcal{C}^T d_{temp}$ 
endif
for  itrace = all receivers for each source
    for   $\mathbf{x} = \text{all } (x, y, z) \text{ positions of earth model}$ 
        for   $\theta = \text{all reflection angles less than maximum aperture}$ 
            read Green's functions table (amplitude, time) from file
            if  forward operator, then
                create data from angle dependent reflectivity:
                 $d_{temp}(\text{itrace}, \text{time}) = \mathcal{L}R(\mathbf{x}, \theta)$ 
            elseif  adjoint operator, then
                create angle dependent reflectivity from data:
                 $\hat{R}(\mathbf{x}, \theta) = \mathcal{L}^T d_{temp}(\text{itrace}, \text{time})$ 
            endif
        endfor
    endfor
endfor
if  forward operator, then
    multiply wavelet with data:  $d_{temp} = \mathcal{C}d_{temp}$ 
    multiply signature and inverse fast Fourier transform data:

```

```
 $d = \text{real}\{\text{ifft}[d_{temp} * S(\omega)]\}$   
endif
```

2.6 Summary

In this chapter, the basic wave equation for scattering problem is derived based on generalized Newton's and Hooke's laws. This non-linear scattering problem is linearized by taking advantage of the Kirchhoff approximation. The linearized solution of the wave equation can be used to further recover the earth image.

Based on the linearized integral, an asymptotic inverse solution is found with the generalized Radon theory (Bleistein and Gray, 2002b).

Chapter 3

Forward/adjoint operators for rock property inversion

3.1 Introduction

Reflection and transmission of seismic waves have been studied significantly for retrieving rock properties from angle dependent reflectivity. The earliest researches about this topic were done in nineteenth century (Green, 1839; Knott, 1899). Zoeppritz (1919) deduced a set of equations to compute the amplitudes of reflected and transmitted waves, and successfully being used in tomographic inversion for calculating reflection and transmission coefficients (Wang, 1999). However, the inversion problem, which estimates elastic parameters from angle dependent reflectivity using Zoeppritz equations, still is a difficult problem. Fortunately, after many laborious exercises, Koefoed (1955) predicted that there would be an invertible relationship between angle dependent coefficient and medium parameters. Koefoed's prediction was realized by many later geophysicists (Bortfeld, 1961; Aki and Richards, 1980; Shuey, 1985; Fatti et al., 1994; Wang, 1999). Although those approximations differ in accuracy, medium, and wavefield parameterizations. All of them are based on the same assumption (Rüger, 2002).

1. The media on both sides of the reflecting boundary have similar elastic properties, and the relative changes in the P- and S-wave velocities and densities across the interface are small.

3.2. A&R APPROXIMATION TO THE ZOEPPRITZ EQUATIONS

2. The incidence angle is sufficiently smaller than the critical angle. At the critical angle, the amplitudes change abruptly and phase changes make any parameter extraction difficult.

Among all approximations, the classic representation was derived by Aki and Richards's (A&R). Their approximation to Zoeppritz equation is always used or further simplified by others. Therefore, I focus on A&R approximation as forward processing to estimate rock properties.

Although A&R approximations are derived for plane waves, they can be used for spherical waves. The reasons are: for far source spherical wave, the wavefront can be approximated locally by plane surface. For near source spherical wave, the wave can be decomposed into a sum of plane waves, and approximation operators can be applied to each plane wave.

In this chapter, I present A&R approximations for P-wave reflection coefficients. Base on this equation, then the forward and adjoint operators are defined. Obviously, I only show the summary of the most important approximated equation to my thesis. Details about the Zoeppritz equations and its approximation can be found in Aki and Richards (1980).

3.2 A&R approximation to the Zoeppritz equations

Reflection and transmission will occur when waves propagate in a discontinuous medium. The elementary formulas for reflection/transmission coefficients can be derived by using kinematic and dynamic boundary conditions. The kinematic boundary condition assumes that displacements are continuous through the boundary, the dynamic boundary condition is the continuity of traction across the interface. Based on these two boundary conditions, the exact formulae for P-P wave¹ reflection coefficients can be expressed in terms of the ray parameter p (Aki and Richards,

¹P-P wave refers to the wave style that both incident wave and reflected wave are P-wave.

1980)

$$\dot{P}\acute{P} = \frac{(b\frac{\cos i_1}{v_{p1}} - c\frac{\cos i_2}{v_{p2}})F - (a + d\frac{\cos i_1}{v_{p1}}\frac{\cos j_2}{v_{s2}})Hp^2}{D}. \quad (3.2.1)$$

Where \dot{P} , and \acute{P} represent incident, and reflected P-wave respectively, and

$$\begin{aligned} a &= \rho_2(1 - 2v_{s2}^2p^2) - \rho_1(1 - 2v_{s1}^2p^2), \\ b &= \rho_2(1 - 2v_{s2}^2p^2) + 2\rho_1v_{s1}^2p^2, \\ c &= \rho_1(1 - 2v_{s1}^2p^2) + 2\rho_2v_{s2}^2p^2, \\ d &= 2(\rho_2v_{s2}^2 - \rho_1v_{s1}^2), \end{aligned}$$

$$\begin{aligned} F &= b\frac{\cos j_1}{v_{s1}} + c\frac{\cos j_2}{v_{s2}}, \\ H &= a - d\frac{\cos i_2}{v_{p2}}\frac{\cos j_1}{v_{s1}}, \\ D &= \frac{\det \mathbf{M}}{v_{p1}v_{p2}v_{s1}v_{s2}}, \end{aligned}$$

with ρ_1 , v_{p1} , and v_{s1} being upper layer's density, P-wave velocity, and S-wave velocity respectively, ρ_2 , v_{p2} , and v_{s2} being lower layer's density, P-wave velocity, and S-wave velocity respectively (Figure 3.1), i_1 , i_2 referring to P-wave incident/reflected and transmitted angle respectively, and j_1 , j_2 representing S-wave reflected, transmitted angle respectively, ray parameter p denoting as

$$p = \frac{\sin i_1}{v_{p1}} = \frac{\sin j_1}{v_{s1}},$$

and the coefficient matrices \mathbf{M} defining as

$$\mathbf{M} = \begin{pmatrix} -v_{p1}p & -\cos j_1 & v_{p2}p & \cos j_2 \\ \cos i_1 & -v_{s1}p & \cos i_2 & -v_{s2}p \\ 2\rho_1v_{s1}^2p \cos i_1 & \rho_1v_{s1}(1 - 2v_{s1}^2p^2) & 2\rho_2v_{s2}^2p \cos i_2 & \rho_2v_{s2}(1 - 2v_{s2}^2p^2) \\ -\rho_1v_{p1}(1 - 2v_{s1}^2p^2) & 2\rho_1v_{s1}^2p \cos j_1 & \rho_2v_{p2}(1 - 2v_{s2}^2p^2) & -2\rho_2v_{s2}^2p \cos j_2 \end{pmatrix}$$

One can see that above expressions are very complex. Rock properties (i.e. ρ , v_p , and v_s) inversion seems to be a 'mission impossible'. Fortunately, under the assumption on page 24, Aki and Richards (1980) approximated above equations as

$$\dot{P}\acute{P} = \frac{1}{2}(1 - 4\frac{v_s^2}{v_p^2} \sin^2 i)\frac{\Delta\rho}{\rho} + \frac{\sec^2 i}{2}\frac{\Delta v_p}{v_p} - \frac{4v_s^2}{v_p^2} \sin^2 i \frac{\Delta v_s}{v_s}, \quad (3.2.2)$$

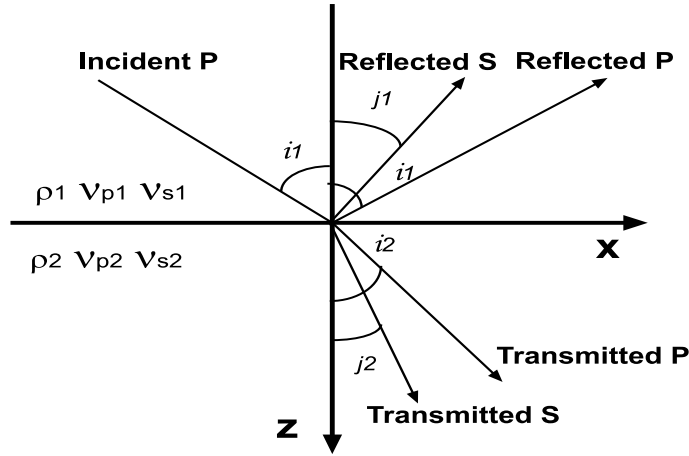


Figure 3.1: Coordinates for analysis of reflected wave set up by a plane P-wave incident on an interface between two solids.

where the elastic properties are:

$$\begin{aligned} \Delta v_s &= v_{s2} - v_{s1}, \\ v_s &= (v_{s2} + v_{s1})/2, \\ \Delta v_p &= v_{p2} - v_{p1}, \\ v_p &= (v_{p2} + v_{p1})/2, \\ \Delta \rho &= \rho_2 - \rho_1, \\ \rho &= (\rho_2 + \rho_1)/2, \\ i &= (i_1 + i_2)/2. \end{aligned}$$

Since this approximation is derived from the assumption of small percentage changing in elastic properties, the difference between incident angle i_1 and transmitted angle i_2 will be small. Therefore, the reflection angle θ can be approximated as the angle i showed above.

3.3 Modeling operators for A&R approximation

As mention in section 2.5 on page 18, the discrete inversion needs the forward and adjoint modeling operators. However, the angle dependent reflectivity is still

3.3. MODELING OPERATORS FOR A&R APPROXIMATION

nonlinear to $\frac{\Delta\rho}{\rho}$, $\frac{\Delta v_p}{v_p}$, and $\frac{\Delta v_s}{v_s}$ in the equation (3.2.2). This is because that the unknown $\frac{v_s}{v_p}$ is a nonconstant coefficient, but function of rock physical parameters. One simplification assumes that the ratio of v_s to v_p is constant² (Wiggins et al., 1983)

$$\frac{v_s}{v_p} = 1/2. \quad (3.3.1)$$

Substituting equation (3.3) to equation (3.2.2), one obtains

$$R(\mathbf{x}, \theta) = \frac{1}{2}(1 - \sin^2 \theta) \frac{\Delta\rho}{\rho} + \frac{\sec^2 \theta}{2} \frac{\Delta v_p}{v_p} - \sin^2 \theta \frac{\Delta v_s}{v_s}, \quad (3.3.2)$$

where \mathbf{x} is any point on the interface, and θ refers to the reflection angle.

3.3.1 Forward modeling

The linear approximated equation can be used to calculate the angle dependent reflectivity for a known elastic interface. The equation (3.3.2) can be expressed as a linear operator \mathcal{Z}

$$R(\mathbf{x}, \theta) = \mathcal{Z}f(\mathbf{x}) \quad (3.3.3)$$

where $f(\mathbf{x})$ represents elastic parameters matrix or vector composed of $\frac{\Delta\rho}{\rho}$, $\frac{\Delta v_p}{v_p}$, and $\frac{\Delta v_s}{v_s}$, $R(\mathbf{x}, \theta)$ is the synthetic angle dependent reflectivity. The linear approximated operator denotes

$$(\mathcal{Z}f)(\mathbf{x}) = \frac{1}{2}(1 - \sin^2 \theta) \frac{\Delta\rho}{\rho} + \frac{\sec^2 \theta}{2} \frac{\Delta v_p}{v_p} - \sin^2 \theta \frac{\Delta v_s}{v_s}. \quad (3.3.4)$$

As working with discrete geophysical data, the linear operator (equation 3.3.4) can be thought of as matrices, and the parameters as vectors or matrices. The discrete forward problem³ is expressed as

$$\begin{pmatrix} R(\theta_1) \\ R(\theta_2) \\ \vdots \\ R(\theta_n) \end{pmatrix} = \begin{pmatrix} \frac{1}{2}(1 - \sin^2 \theta_1) & \frac{\sec^2 \theta_1}{2} & -\sin^2 \theta_1 \\ \frac{1}{2}(1 - \sin^2 \theta_2) & \frac{\sec^2 \theta_2}{2} & -\sin^2 \theta_2 \\ \vdots & \vdots & \vdots \\ \frac{1}{2}(1 - \sin^2 \theta_n) & \frac{\sec^2 \theta_n}{2} & -\sin^2 \theta_n \end{pmatrix} \begin{pmatrix} \frac{\Delta\rho}{\rho} \\ \frac{\Delta v_p}{v_p} \\ \frac{\Delta v_s}{v_s} \end{pmatrix}. \quad (3.3.5)$$

²Other experimental approximations can be used depending on local rock physical condition for real data.

³To be simple, this expression is only for one reflection point in space.

3.3.2 Adjoint modeling

As defined in section 2.5.2 on page 19, the adjoint operator can be obtained by taking the transpose of the forward matrix. Thus, the adjoint modeling operator is

$$\hat{f}(\mathbf{x}) = \mathcal{Z}^T R(\mathbf{x}, \theta) \quad (3.3.6)$$

where $\hat{f}(\mathbf{x})$ is the result obtained by applying the adjoint operator to the model.

As mentioned above, when working with discrete expression of the model and data, the adjoint operators are implemented as matrices. Equation (3.3.6) can be expressed as

$$\begin{pmatrix} \frac{\hat{\Delta}\rho}{\rho} \\ \frac{\hat{\Delta}v_p}{v_p} \\ \frac{\hat{\Delta}v_s}{v_s} \end{pmatrix} = \begin{pmatrix} \frac{1}{2}(1 - \sin^2 \theta_1) & \frac{1}{2}(1 - \sin^2 \theta_2) & \dots & \frac{1}{2}(1 - \sin^2 \theta_n) \\ \frac{\sec^2 \theta_1}{2} & \frac{\sec^2 \theta_2}{2} & \dots & \frac{\sec^2 \theta_n}{2} \\ -\sin^2 \theta_1 & -\sin^2 \theta_2 & \dots & -\sin^2 \theta_n \end{pmatrix} \begin{pmatrix} R(\theta_1) \\ R(\theta_2) \\ \vdots \\ R(\theta_n) \end{pmatrix}. \quad (3.3.7)$$

3.4 Implementation of modeling operators

A&R approximation operators can be completed by matrices operation. In order to combine with the Kirchhoff modeling processing, the subroutines operators are defined to perform A&R approximation processing.

The pseudo-code for the subroutine is given below. The subroutine named *AER_for_adj* is for an earth model.

```
# Subroutine for AER forward/adjoint modeling operators
for    $\mathbf{x}$  = all (x, y, z) positions of earth model
      for    $\theta$  = all reflection angles less than maximum aperture
            if   forward operator, then
                  create angle dependent reflectivity from elastic model:
                   $R(\mathbf{x}, \theta) = \mathcal{Z}f(\mathbf{x})$ 
            elseif   adjoint operator, then
```

create model from angle dependent reflectivity:

$$\hat{f}(\mathbf{x}) = \mathcal{Z}^T R(\mathbf{x}, \theta)$$

endif

endfor

endfor

3.5 Integrating AVA inversion with Kirchhoff migration

In the Chapter 2, I reviewed the linear scattering problem

$$d = \mathcal{C}\mathcal{L}R(\mathbf{x}, \theta). \tag{3.5.1}$$

Note that the angle dependent reflectivity $R(\mathbf{x}, \theta)$ is related to the vector of physical parameters $f(\mathbf{x})$ via a Zoeppritz forward operator

$$R(\mathbf{x}, \theta) = \mathcal{Z}f(\mathbf{x}) \tag{3.5.2}$$

Therefore, combining equation 3.5.1 and equation 3.5.2, the seismic data can now be expressed by

$$d = \mathcal{C}\mathcal{L}\mathcal{Z}f(\mathbf{x}). \tag{3.5.3}$$

and its adjoint operator can be written as

$$\hat{f}(\mathbf{x}) = \mathcal{Z}^T \mathcal{L}^T \mathcal{C}^T d. \tag{3.5.4}$$

Our inverse algorithm is based on the equation 3.5.3 and equation 3.5.4⁴ By means of the CG, we can easily obtain the perturbation of rock properties $f(\mathbf{x})$. The common image gather $R(\mathbf{x}, \theta)$ is generated by substituting the inverted rock physical parameters back to the A&R approximation to the Zoeppritz equation.

⁴Actually, the three variables of $f(\mathbf{x})$ are correlated (Downton and Lines, 2001). The algorithm presented here does not included a model covariance matrix. Including correlation among parameters is a non-trivial problem since these parameters are unknown.

3.6 Summary

In this chapter, the A&R approximation of P-wave's reflectivity is presented for Zoeppritz equations. Using kinematic and dynamic boundary conditions, the approximation leads a way to retrieval rock properties from CIGs in angle domain efficiently. In order to linearize A&R approximation to elastic parameters $\frac{\Delta\rho}{\rho}$, $\frac{\Delta v_p}{v_p}$, and $\frac{\Delta v_s}{v_s}$, the assumption $\frac{v_s}{v_p} = 1/2$ is used, which was derived by Wiggins et al. (1983).

To simplify the problem, the forward processing operators of A&R approximation are derived for plane wave. Since a relative large radius of a spherical wave can be approximated locally by a plane surface. Moreover, spherical wave can be decomposed into a sum of plane wave, and the operators can be applied to each plane wave individually. Therefore, the operators can still be used for spherical waves.

The forward and adjoint operators are derived from the linearized A&R approximation. In keeping with the previous algorithm, the discrete operators are performed with subroutines. This enables combination of two parallel operators, Kirchhoff and A&R approximation operators, together to invert rock properties directly from pre-stack seismic data.

Chapter 4

Inversion of angle gathers and rock properties

4.1 Introduction

Seismic inversion is the processing which determines the characteristics of the interior of the earth based on observations from a surface. It is the reverse calculation of the forward problem. Generally, perfect data¹ will give perfect inverted result (Claerbout, 1992). But seismic data are incomplete and inaccurate. In order to avoid dividing by zero, many geophysicists replace inversion with migration (or adjoint processing). However, the migrated result can not recover amplitude information, which is important for AVA/AVO analysis. Moreover, the adjoint operators treat missing data as assuming they are zero-valued data, which further limit the resolution. Fortunately, since adjoint processing is the first step of inversion (Tarantola, 1984; Claerbout, 1992). The inversion can be approached by using forward and adjoint operators iteratively. Such numerical method is called discrete inversion.

Discrete inversion technique finds the solution by minimizing the cost function (Tarantola, 1987; Jin et al., 1992; Thierry et al., 1999), which is composed by two parts: one is l_2 norm misfit — difference between the observed data and the predicted data from the earth model; another is the regularization terms which force

¹Perfect data are noise free data, and contain enough information to evaluate all of the rock physical properties within every cell of a tomographic grid.

the solution toward the desired characteristics. Usually, the regularization terms are defined in terms of l_1 and l_2 norms.

In this chapter, I present the basic idea and formulas of discrete inversion theory. Then, the forward and adjoint operators for rock properties inversion are defined and finally, an inversion methodology is proposed.

4.2 Discrete inversion theory

Geophysical data are discretely recorded with regular or irregular time/space samples. Thus, the data can be expressed as matrices or vectors. Moreover, the word "inversion" originally come from "matrix inversion" (Claerbout, 1992). Therefore, the linear operator can be thought of as matrices.

4.2.1 Seismic discrete inversion problem

Retrieving approximated rock properties from a pre-stack data set can be regarded as linear inverse problem

$$\mathbf{d} = \mathbf{G}\mathbf{m} + \mathbf{n}, \tag{4.2.1}$$

where \mathbf{d} refers to the pre-stack data defined as a vector of $(d_1, d_2, \dots, d_N)^T$, N is the number of observation data, \mathbf{m} refers to the model defined as a vector of $(m_1, m_2, \dots, m_M)^T$, M is the number of unknowns of the model, \mathbf{n} represents additive noise that we assume Gaussian, and \mathbf{G} represents the matrix operator defined as

$$\begin{pmatrix} G_{11} & G_{12} & \dots & G_{1M} \\ G_{21} & G_{22} & \dots & G_{2M} \\ \vdots & \vdots & \ddots & \vdots \\ G_{N1} & G_{N2} & \dots & G_{NM} \end{pmatrix}.$$

Since there is no way to collect reflected data from each small tomographic grid within the earth. Usually, the number of data N is smaller than the number of unknowns M . Therefore, the inverse problem (equation 4.2.1) will have more than one solution. In order to resolve such an ill-posed problem, a constrained least squares approach is used.

The least squares approach finds the solution by minimizing error or distance between synthetic and original data. The distance is equivalent to following objective or cost function

$$\mathcal{J}(\mathbf{m}) = \mathbf{e}^T \mathbf{e} = (\mathbf{d} - \mathbf{G}\mathbf{m})^T (\mathbf{d} - \mathbf{G}\mathbf{m}) = \|\mathbf{d} - \mathbf{G}\mathbf{m}\|_2^2. \quad (4.2.2)$$

To obtain the minimum of the cost function, the derivative of the function (equation 4.2.2) with respect to the model parameters is set to zero

$$\frac{\partial \mathcal{J}(\mathbf{m})}{\partial \mathbf{m}} = \frac{\partial (\mathbf{d} - \mathbf{G}\mathbf{m})^T (\mathbf{d} - \mathbf{G}\mathbf{m})}{\partial \mathbf{m}} = 0, \quad (4.2.3)$$

after some manipulations, one obtains

$$\tilde{\mathbf{m}} = (\mathbf{G}^T \mathbf{G})^{-1} \mathbf{G}^T \mathbf{d}, \quad (4.2.4)$$

where $\tilde{\mathbf{m}}$ are the recovered model parameters. $\mathbf{G}^T \mathbf{d}$ denotes adjoint (or the gradient of the cost function). $\mathbf{G}^T \mathbf{G}$ is the Hessian.

In geophysical inverse problem, the Hessian is a huge matrix². We will face a daunting computation for the inversion of the Hessian if we use this equation to invert the model parameters³. This is why we will directly operate on the minimization of the cost function using the method of conjugate gradients (CG). In other words we will avoid forming the inverse of $\mathbf{G}^T \mathbf{G}$ ⁴. A good review of the CG method and application to geophysical inverse problems can be found in Scales (1987).

It is important to distinguish migration and inversion. As mentioned above, migration is the gradient at first iteration of a local optimization (Tarantola, 1984).

²For example, a 2D pre-stack seismic data, the number of elements of Hessian is $(N_s \times N_r \times N_t)^2$, it would be more than trillions, where N_s , N_r , N_t represent number of source, receiver, and time sample respectively

³The computation of inverting a $N \times N$ matrix is N^3 , but CG only $K \times N^2$ with K being number of iteration, and $N \gg K$.

⁴This is a task only feasible for small 1D problems

To be clear

$$\begin{aligned}
\tilde{\mathbf{m}} &= (\mathbf{G}^T \mathbf{G})^{-1} \mathbf{G}^T \mathbf{d} \\
&= \mathbf{G}^\dagger \mathbf{d} \quad \text{inversion,} \\
\end{aligned} \tag{4.2.5}$$

$$\hat{\mathbf{m}} = \mathbf{G}^T \mathbf{d} \quad \text{migration.}$$

Obviously, if $\mathbf{G}^T \mathbf{G} = \mathbf{I}$, where \mathbf{I} is used to indicate the identity operator, the inversion is precisely estimated by the migration. In seismic application, unfortunately, this situation seldom occurs.

Applied to perfect data, inversion will give perfect result. This is why that inversion is more appealing academically than migration. However, it is also important for us to know the limitation of the inverse operator \mathbf{G}^\dagger

$$\begin{aligned}
\tilde{\mathbf{m}} &= \mathbf{G}^\dagger \mathbf{d} \\
&= (\mathbf{G}^T \mathbf{G})^{-1} \mathbf{G}^T \mathbf{d} \\
&= (\mathbf{G}^T \mathbf{G})^{-1} \mathbf{G}^T \mathbf{G} \mathbf{m} \\
&= \mathbf{G}^\dagger \mathbf{G} \mathbf{m}.
\end{aligned} \tag{4.2.6}$$

Clearly, if $\mathbf{G}^\dagger \mathbf{G} = (\mathbf{G}^T \mathbf{G})^{-1} \mathbf{G}^T \mathbf{G} = \mathbf{I}$. The inverted image equals to the *true* image of the subsurface. In general, noise and the inherent problem of operator mismatch precludes us of attempting to find an exact inverse to the operator \mathbf{G} . We simply consider the solution where $\mathbf{G}^\dagger \mathbf{G} \approx \mathbf{I}$, in other words, the inverted image $\tilde{\mathbf{m}}$ should offer some improvements with respect to the migrated result $\hat{\mathbf{m}}$, and a good approximation to the true image \mathbf{m} . Figure 2.3 shows a good example for the above statement.

4.2.2 Constraints

As mentioned above, the geophysical problems (equation 4.2.1) are ill-posed. Thus, the matrix $\mathbf{G}^T \mathbf{G}$ in equation (4.2.4) is in general unstable or not invertible. In order to retrieve a stable, unique solution from noisy and incomplete data, constraints are

applied to force a desired solution. Hence, a new cost function is formed by a data misfit term and a constraint term

$$\mathcal{J}(\mathbf{m}) = \|\mathbf{d} - \mathbf{G}\mathbf{m}\|_2^2 + \mu\|R(\mathbf{m})\|_l^l. \quad (4.2.7)$$

Where regularization term $R(\mathbf{m})$ is expressed as an l norm (i.e., l_1 or l_2 norm), and μ denotes the trade-off parameter, which defines the priority given to satisfying the constraint versus the data misfit term.

The trade-off parameter affects the solution greatly. If the trade-off parameter is set to zero, the solution will totally fit the data. Inversely, when the trade-off parameter approaches infinity, all efforts will be put toward minimizing the regularization term and the solution will not fit the data. Thus, to retrieve a realistic solution, the optional trade-off parameter must be a compromise to satisfy both terms. The details for determining trade-off parameters, please see Youzwishen (2001).

The desirable solution can be obtained by minimizing the cost function (equation 4.2.7)

$$\frac{\partial \mathcal{J}(\mathbf{m})}{\partial \mathbf{m}} = 2\mathbf{G}^T \mathbf{G}\mathbf{m} - 2\mathbf{G}^T \mathbf{d} + 2\mu \mathbf{Q}_m^T \mathbf{Q}_m \mathbf{m} = 0, \quad (4.2.8)$$

after some manipulations, one obtains

$$\tilde{\mathbf{m}} = (\mathbf{G}^T \mathbf{G} + \mu \mathbf{Q}_m^T \mathbf{Q}_m)^{-1} \mathbf{G}^T \mathbf{d}. \quad (4.2.9)$$

where \mathbf{Q}_m is derived from the regularization term $\|R(\mathbf{m})\|_l$

$$\mathbf{Q}_m^T \mathbf{Q}_m = \frac{1}{2} \frac{\partial \|R(\mathbf{m})\|_l^l}{\partial \mathbf{m}}$$

The same as the equation (4.2.4), the equation (4.2.9) need to calculate the Hessian $\mathbf{G}^T \mathbf{G}$. To make calculation efficiently, the CG algorithm is used for such constrained least squares inversion.

Usually, there are two kinds of constraints, quadratic constraints expressed in l_2 norm and non-quadratic constraints expressed, for instance, with an l_1 norm. Quadratic constraints result in a linear inverse problem. This is because the matrix \mathbf{Q}_m in equation (4.2.9) is not the function of the model \mathbf{m} . Non-quadratic

constraints result in a nonlinear inverse problem. However, many geophysicists proposed algorithms which solve the l_1 norm non-quadratic constraints problem in a linear, iterative manner (Scale and Smith, 1994; Sacchi, 1997; Youzwishen, 2001).

Quadratic constraints

Since most structures of the earth vary continuously along horizontal direction, the common quadratic constraint is to enforce a continuous solution (Youzwishen, 2001; Duquet et al., 2000). The simplest one of such continuous solution is a flat solution that has little change between adjacent parameters.

The flat solution can be obtained by minimizing the first derivative of the model norm.

$$\mathbf{m}' = \frac{\partial \mathbf{m}}{\partial x} \approx \frac{m_{i+1} - m_i}{\Delta x}. \quad (4.2.10)$$

Obviously, the derivative in above equation can be estimated by convolution with the filter $(1, -1)/\Delta x$. Thus, The equation (4.2.10) can be rewritten as weighting matrices \mathbf{D}_1 which act on the vector of model parameters \mathbf{m}

$$\mathbf{D}_1 \mathbf{m} = \frac{1}{\Delta x} \begin{pmatrix} 1 & -1 & 0 & \dots & 0 \\ 0 & 1 & -1 & \dots & 0 \\ \vdots & \vdots & \ddots & \ddots & \vdots \\ 0 & \dots & 0 & 1 & -1 \\ 0 & \dots & 0 & 0 & 1 \end{pmatrix} \begin{pmatrix} m_1 \\ m_2 \\ \vdots \\ m_{M-1} \\ m_M \end{pmatrix}.$$

Applying the flat regularization term to the cost function, the solution can be obtained by replacing the weighting matrix of equation (4.2.9) with the derivative matrix \mathbf{D}_1

$$\tilde{\mathbf{m}} = (\mathbf{G}^T \mathbf{G} + \mu \mathbf{D}_1^T \mathbf{D}_1)^{-1} \mathbf{G}^T \mathbf{d}. \quad (4.2.11)$$

Where the transpose matrix \mathbf{D}_1^T is defined as

$$\mathbf{D}_1^T = \begin{pmatrix} 1 & 0 & 0 & \dots & 0 \\ -1 & 1 & 0 & \dots & 0 \\ \vdots & \ddots & \ddots & \vdots & \vdots \\ 0 & \dots & -1 & 1 & 0 \\ 0 & \dots & 0 & -1 & 1 \end{pmatrix}$$

The smooth convolution matrices (\mathbf{D}_1 and \mathbf{D}_1^T) showed above are only for one dimensional problem. In two (2D) or three (3D) dimensional problems, the matrix of parameters will be rewritten in lexicographic order. The derivative matrices for such cases will be determined by model parameters which are adjacent in the vector \mathbf{m} . For example, a model parameters panel of a 2D problem can be written as

$$\begin{pmatrix} m_{11} & m_{12} & \dots & m_{1n_x} \\ m_{21} & m_{22} & \dots & m_{2n_x} \\ \vdots & \vdots & \ddots & \vdots \\ m_{n_z 1} & m_{n_z 2} & \dots & m_{n_z n_x} \end{pmatrix} \rightarrow \begin{pmatrix} m_{11} \\ m_{12} \\ \vdots \\ m_{1n_x} \\ m_{21} \\ m_{22} \\ \vdots \\ m_{2n_x} \\ \vdots \\ m_{n_z 1} \\ m_{n_z 2} \\ \vdots \\ m_{n_z n_x} \end{pmatrix}$$

with n_x, n_z being number of samples along the horizontal and the vertical direction respectively. The smooth convolution matrices applied for the horizontal and the vertical directions are

$$\mathbf{D}_x = \begin{pmatrix} \mathbf{D}_{x1} & & & \\ & \mathbf{D}_{x2} & & \mathbf{0} \\ & & \mathbf{D}_{x3} & \\ & \mathbf{0} & & \ddots \\ & & & & \mathbf{D}_{xn_z} \end{pmatrix},$$

and

$$\mathbf{D}_z = \begin{pmatrix} \mathbf{D}_{z1} & & & \\ & \mathbf{D}_{z2} & & \mathbf{0} \\ & & \mathbf{D}_{z3} & \\ & \mathbf{0} & & \ddots \\ & & & & \mathbf{D}_{zn_x} \end{pmatrix}$$

respectively, where

$$\mathbf{D}_{x1} = \mathbf{D}_{x2} = \cdots = \mathbf{D}_{xn_x} = \underbrace{\begin{pmatrix} 1 & -1 & & & \\ & 1 & -1 & & \mathbf{0} \\ & & \ddots & \ddots & \\ & \mathbf{0} & & 1 & -1 \\ & & & & 1 \end{pmatrix}}_{\text{total number is } n_x},$$

$$\mathbf{D}_{z1} = \mathbf{D}_{z2} = \cdots = \mathbf{D}_{zn_x-1} = \underbrace{\begin{pmatrix} 1 & \overbrace{n_x-1 \text{ numbers of zero}}^{\dots} & & -1 & & \\ & 1 & & \dots & -1 & \mathbf{0} \\ & & \ddots & & & \\ & \mathbf{0} & & & 1 & \dots & -1 \end{pmatrix}}_{\text{total number is } 2 \times n_x},$$

$$\mathbf{D}_{zn_x} = \underbrace{\begin{pmatrix} 1 & & & \\ & 1 & & \mathbf{0} \\ & \mathbf{0} & \ddots & \\ & & & 1 \end{pmatrix}}_{\text{total number is } n_x}.$$

Non-quadratic constraints

The most common non-quadratic regularization term is the l_1 norm. Unlike smoothing terms, sparseness will preserve edges and discontinuities along faults, and increase vertical resolution (Sacchi et al., 2003). When sparseness is enforced on a model parameter, the resulting solution will be spiky. In the same vein, as sparseness is enforced on the first derivative of a model parameter, the resulting solution will be blocky.

Since this thesis focuses on AVA and variation of rock properties inversion, I mainly discuss the spiky regularization term. It is defined as

$$R(\mathbf{m}) = \sum_{i=1}^M |m_i|. \quad (4.2.12)$$

Substituting equation (4.2.12) into equation (4.2.7), and minimizing this cost function, after some manipulations, one obtains

$$2\mathbf{G}^T\mathbf{G}\mathbf{m} - 2\mathbf{G}^T\mathbf{d} + \mu\mathit{sign}(\mathbf{m}) = 0. \quad (4.2.13)$$

where $\mathit{sign}(m_i) = \frac{m_i}{|m_i|}$. Subsequently,

$$\tilde{\mathbf{m}} = [\mathbf{G}^T\mathbf{G} + \frac{\mu}{2}\mathit{sign}(\mathbf{m})\mathbf{m}^{-1}]^{-1}\mathbf{G}^T\mathbf{d}. \quad (4.2.14)$$

Obviously, this equation is nonlinear. Because the solution is the function of itself, in order to solve it with CG, let's rewrite the spiky regularization term

$$\begin{aligned} R(\mathbf{m}) &= \sum_{i=1}^M \left| \frac{m_i}{\sqrt{|m_i|}} \right|^2 \\ &= \|\mathbf{Q}_m\mathbf{m}\|_2^2 \end{aligned} \quad (4.2.15)$$

where \mathbf{Q}_m is the diagonal matrix defined in terms of the vector \mathbf{m}

$$\mathbf{Q}_m = \begin{pmatrix} \frac{1}{\sqrt{|m_1|}} & & & & \\ & \frac{1}{\sqrt{|m_2|}} & & & \\ & & \frac{1}{\sqrt{|m_3|}} & & \\ & & & \ddots & \\ & & & & \frac{1}{\sqrt{|m_M|}} \end{pmatrix} \quad (4.2.16)$$

To avoid divided by zero, we often replace the unknowns in equation (4.2.16) by

$$\frac{1}{\sqrt{|m_1|}} \rightarrow \frac{1}{\sqrt{|m_1| + \epsilon}}, \quad (4.2.17)$$

where ϵ is a small positive number.

By defining a new spiky constraint operator as equation (4.2.16) and equation (4.2.17), the l_1 norm function (equation 4.2.12) is rewritten as an l_2 norm function (equation 4.2.15). Thus, the weakly nonlinear problem (equation 4.2.13) can be solved by using the iteratively re-weighted least squares technique in a linear, iterative manner (Scale and Smith, 1994).

4.3 Constrained least-squares migration/inversion

As mentioned above, in order to avoid forming matrix $\mathbf{G}^T\mathbf{G}$, the cost function itself is used to find a solution. Therefore, numerical optimization techniques are used for minimizing the cost function iteratively. We minimize the following cost function:

$$\mathcal{J}(\mathbf{m}) = \|\mathbf{d} - \mathbf{G}\mathbf{m}\|_2^2 + \lambda\|R_{sm}(\mathbf{m})\|_2^2 + \mu\|R_{sp}(\mathbf{m})\|_2^2. \quad (4.3.1)$$

where R_{sm} represents smoothness constraint described in subsection 4.2.2, R_{sp} denotes sparseness constraint described in subsection 4.2.2. λ , and μ are tradeoff parameters.

In the cost function showed above, the smoothness constraint and the sparseness constraint seem to be in conflict in some sense. As smoothness constraint enforces smoothness and penalizes discontinuities and rapid parameters changes. At the same time, the sparseness constraint enforces the discontinuities. However, giving the proper weights (tradeoff parameters) for those two operators, the promised result will be smoothed or discontinued at the area where it should be. Therefore, such cost function is suitable for retrieving earth's properties. Usually in the earth, along the horizontal direction, faults cut off the continuity of the background. Along the vertical direction, rock properties are continuous in the layers, and discontinuous between the layers.

Iterative gradient minimization by conjugate gradients (CG) is one of the best methods for geophysical inverse problems. There are two advantages of using CG minimization for seismic inversion. First, CG minimization approaches the desired solution by repeating forward/adjoint-type processes. Thus, it avoids inverting the product $\mathbf{G}^T\mathbf{G}$ directly. This is very important for seismic inverse problems. In fact, seismic forward and adjoint operators are coded as functions rather than matrices. Second, CG minimization is an efficient way for the seismic inversion because it is $\frac{N}{K}$ times faster than traditional Gaussian elimination methods, where N is the dimension of the inverted matrix and K is the number of iterations, and $N \gg K$.

4.3.1 Conjugate gradients implementation

The pseudo-code for the subroutine of CG is given below. The subroutine named *CG_operator*. Details about the CG algorithm can be found in Claerbout (1992), Strang (1986), and especially Scale (1987).

```
# Subroutine for CG algorithm
# initialization
r = d           # d represents the data
m = m0       # m refers to the model
# calculating gradient
p = GTr
s = p
q = Gp
# begin iteration
for iter = 1, max_iteration
     $\alpha' = \mathbf{s}^T \mathbf{s}$ 
     $\alpha = \frac{\alpha'}{\mathbf{q}^T \mathbf{q}}$ 
    m = m +  $\alpha * \mathbf{p}$            # update model
    r = r -  $\alpha * \mathbf{q}$          # update residual
    s = GTr
     $\beta = \frac{\mathbf{s}^T \mathbf{s}}{\alpha'}$ 
    p = s +  $\beta * \mathbf{p}$ 
    q = Gp
end
```

4.3.2 Forward/adjoint operator for inversion

As shown in section 4.3.1, the CG algorithm includes only one matrix operator **G**, but the cost function on page 41 contains more than one matrix operator. Moreover,

4.3. CONSTRAINED LEAST-SQUARES MIGRATION/INVERSION

the forward operator \mathbf{G} is composed by Kirchhoff and A&R forward operators. For this reason, an integrated matrix (or argumented matrix) operator must be formed. In other words, the reformed cost function with regularization term (equation 4.3.1) should look like the standard cost function (equation 4.2.2). Since the sparseness regularization term can be rewritten in the form of quasi l_2 norm (equation 4.2.15), the cost function can be expressed in quadratic form by substituting the flat constraint operator \mathbf{D}_1 and the spiky constraint operator \mathbf{Q}_m described in the section 4.2.2 into equation (4.3.1)

$$\mathcal{J}(\mathbf{m}) = \|\mathbf{d} - \mathbf{G}\mathbf{m}\|_2^2 + \lambda\|\mathbf{D}_1\mathbf{m}\|_2 + \mu\|\mathbf{Q}_m\mathbf{m}\|_2^2. \quad (4.3.2)$$

The above equation is equivalent to

$$\mathcal{J}(\mathbf{m}) = \|\mathbf{d}_A - \mathbf{G}_A\mathbf{m}\|_2^2, \quad (4.3.3)$$

where \mathbf{d}_A is a new data vector which is composed by padding zeros⁵ to the end of the data vector \mathbf{d}

$$\mathbf{d}_A = \begin{pmatrix} \mathbf{d} \\ \mathbf{0} \end{pmatrix} \quad (4.3.4)$$

and \mathbf{G}_A is the argumented operator

$$\mathbf{G}_A = \begin{pmatrix} \mathbf{G} \\ \sqrt{\lambda}\mathbf{D}_1 \\ \sqrt{\mu}\mathbf{Q}_m \end{pmatrix}, \quad (4.3.5)$$

with the matrix operator \mathbf{G} being denoted as

$$\mathbf{G} = \mathbf{CLZ}, \quad (4.3.6)$$

where \mathbf{CL} forms the Kirchhoff forward operator which is described in section 2.5.1 on page 19, and \mathbf{Z} represents A&R forward operator which is described in section 3.3.1 on page 28.

Substituting equation (4.3.4) and (4.3.5) to equation (4.3.3), and comparing to standard cost function. Finally, one obtains forward operator for such constrained

⁵Numbers of zero are determined by the number of parameters of \mathbf{D}_1 and \mathbf{Q}_m .

least squares inverse problem

$$\begin{pmatrix} \mathbf{d} \\ \mathbf{0} \end{pmatrix} = \begin{pmatrix} \mathbf{CLZ} \\ \sqrt{\lambda}\mathbf{D}_1 \\ \sqrt{\mu}\mathbf{Q}_m \end{pmatrix} \mathbf{m}, \quad (4.3.7)$$

and its adjoint operator

$$\hat{\mathbf{m}} = \begin{pmatrix} \mathbf{Z}^T \mathbf{L}^T \mathbf{C}^T & \sqrt{\lambda}\mathbf{D}_1^T & \sqrt{\mu}\mathbf{Q}_m^T \end{pmatrix} \begin{pmatrix} \mathbf{d} \\ \mathbf{0} \end{pmatrix}. \quad (4.3.8)$$

4.4 Implementation of the inversion algorithm

The desired solution of the inverse problem can be retrieved by the CG algorithm.

The computation steps are listed below (Sacchi, 1997).

1. Initialize the model parameters for rock properties $f(x)$. Most commonly, the default model is set to zero for each parameter if there is not enough information to begin elsewhere.
2. Input Green's function table and macro velocity model. Green's functions are calculated by the target oriented ray tracing method.
3. Select maximum iteration and the tradeoff parameters and e_{max} .
4. Call the CG subroutine. The CG subroutine also calls the Kirchhoff forward/adjoint and A&R forward/adjoint subroutines.
5. During the CG iteration processing, output the result if $\frac{|\mathcal{J}^k - \mathcal{J}^{k-1}|}{(|\mathcal{J}^k| + |\mathcal{J}^{k-1}|)/2} \leq e_{max}$, where \mathcal{J}^k is the cost function evaluated at iteration k .
6. Plot the image and the misfit to determine if the tradeoff parameter need adjustment.

4.5 Summary

In this chapter, I review the discrete inverse theory. An inversion method based on the CG algorithm is proposed. This inverse technique uses the forward and adjoint

operators couple to retrieve the approximated solution iteratively. The advantages of such iterative inverse technique are as follows.

1. The algorithm can be easily coded and efficiently executed.
2. The scheme avoids computed the product $\mathbf{G}^T\mathbf{G}$ which can not be formed for multidimensional geophysical inverse problems.
3. The algorithm does not require large amount of computer memory. The forward and adjoint operators are coded as functions rather than matrices.

Since faults cut off the continuity of the background in the horizontal plane, and rock properties are continuous in the layers but discontinuous between the layers along the vertical direction, the quadratic smoothing constraint is used in the horizontal plane and a non-quadratic sparse constraint is applied to improve the vertical resolution. This technique has been developed by our group in recent years (Feng and Sacchi, 2004a).

Chapter 5

Target oriented ray tracing for Green's function

5.1 Introduction

Due to its flexibility and efficiency, ray based Kirchhoff migration/inversion is more popular than other methods in exploration geophysics. Imaging goals focus now on recovering elastic properties. True amplitude migration for complex media, which is based on a weighted diffraction stack, becomes more and more important. However, the Green's functions (or weighting functions) are computationally expensive. Therefore, an efficient strategy for calculating the Green's functions¹, as well as high accuracy, will significantly reduce the cost of the amplitude-preserving migration.

The Green's functions are composed of two parts: travel times and amplitudes. Generally, the travel time and amplitude can be obtained by ray tracing methods, which mainly consists in solving the two ray equations — eikonal and transport equations. Based on high frequency approximation, usually the seismic ray tracing is used to calculate the rays, travel times, wavefronts (the kinematic aspects of wave propagation, computed by eikonal equation) and amplitudes (dynamic part of the wave propagation, computed by the transport equation).

There are lots of ray tracing methods for calculating the Green's function. The

¹If the source function is an impulse, the solution of the Helmholtz equation is called Green's function, or impulse response.

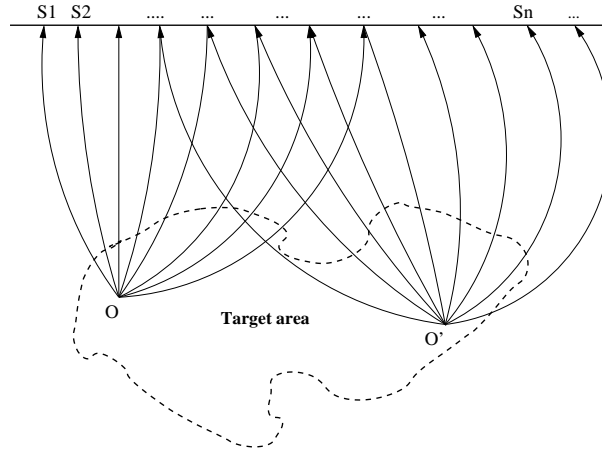


Figure 5.1: Target oriented ray tracing.

classical paper, which is written by Cerveny et al. (1977), forms the foundation of dynamic ray tracing. However, these algorithms are quite expensive. Vanelle (2002) proposed an algorithm based on hyperbolic traveltimes expansion. Because the method uses only kinematic ray tracing, the computational efficiency is increased.

In this Chapter, I propose a target oriented ray tracing for computing the Green's function based on the kinematic ray tracing. Therefore, the algorithm is efficient. Furthermore, our method takes into account all relevant arrivals from all directions by shooting dense up-going rays from the image points. As the angles of the rays are needed for the approximation. I also present the algorithm for computing angle based on the eikonal equation.

5.2 Target oriented ray tracing

Target oriented ray tracing is used to compute the Green's function for the Kirchhoff migration/inversion algorithm (Figure 5.1). The rays are shot from the image points up to the surface. To avoid migration/inversion operator aliasing, the density of the rays are chosen depending on the complexity of the model, the more complex of the model is, the more dense of the rays will be used. Since the ray tracing is only executed in selected image domain at which the interesting targets locate. Therefore,

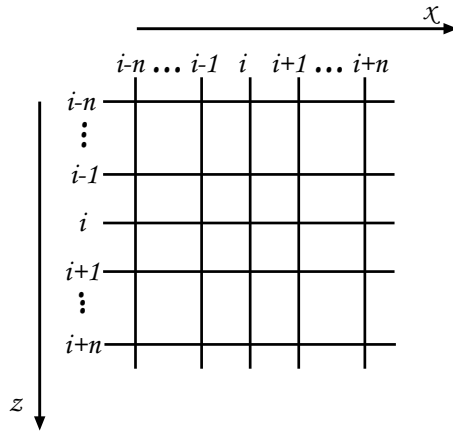


Figure 5.2: Sketch of a filter grid.

it will be efficient and flexible. For example, no acquisition regularity assumption is necessary, and the algorithm can be easily applied on parallel computers.

5.2.1 The macro-velocity model

The ray tracing requires the input of a macro velocity model (or migration velocity model). The macro velocity, which is the low frequency background of the earth model, hence for synthetic data, is obtained from the earth model using a low pass filter. For example, a 2D filter denotes

$$F = \begin{pmatrix} f_{i-n,i-n} & \cdots & f_{i-n,i} & \cdots & f_{i-n,i+n} \\ \vdots & \ddots & \vdots & & \vdots \\ f_{i,i-n} & \cdots & f_{i,i} & \cdots & f_{i,i+n} \\ \vdots & & \vdots & \ddots & \vdots \\ f_{i+n,i-n} & \cdots & f_{i+n,i} & \cdots & f_{i+n,i+n} \end{pmatrix}, \quad (5.2.1)$$

on the condition of

$$\sum_{j,k=-n}^n |f_{i-j,i-k}| = 1.0,$$

where i and n are showed in the Figure 5.2. Usually, I choose $n = 100$ for the filter.

When dealing with real seismic data, we invert the Dix's equation (1955) to

obtain the interval velocities c_i from stacking velocities $C(t)$.

$$C^2(t) = \frac{1}{t} \sum_{i=0}^{N-1} \Delta t_i c_i^2 \quad (5.2.2)$$

where Δt_i is the time interval, and $t = \sum_{i=0}^{N-1} \Delta t_i$.

The inversion of equation 5.2.2 only gives the vertical velocity variation at some CMP locations. The lateral velocity variation can be obtained by any interpolation method between the CMPs.

5.2.2 The Green's function

As mentioned before, the Green's function should be calculated before the Kirchhoff migration/inversion. The Green's function includes amplitude and time information, which is crucial for the Kirchhoff operators. However, calculating the Green's function is troublesome, since there is no analytical expression for complex media. An approximation to the Green's function is created by a modeling scheme that uses the first-guess wave speed profile (Bleistein et al., 2001), or macro/migration velocity model. Such an approximate function can be constructed by finite-difference method (FD) or asymptotic method (Chapter 2). The FD method is more accurate, but expensive. Furthermore, it can not provide the reflection angle information directly, which is important for our proposed AVA inversion algorithm. Unsurprisingly, the asymptotic method has those merits that FD does not have. Therefore, an asymptotic method called ray tracing is used to obtain the Green's function in this thesis.

Seismic ray tracing method mainly consists of solving the two ray equations—eikonal and transport equations. It is an asymptotic approximation to the wave equation that describes the process of propagation of seismic waves in the high frequency regime. Ray tracing can be used to calculate the rays, travel times, wavefronts and amplitudes. Since the traditional dynamic ray tracing is expensive, an approximation for 2D acoustic Green's function is proposed.

5.3 Travel times approximation

The eikonal equation is usually solved by "method of characteristics". More details see Bleistein, et al. (2001) or Kravtson and Orlov (1990). The ray tracing system (kinematic) is composed of six ordinary differential equations. Usually, they are written as following two vectors equation

$$\frac{d\mathbf{x}}{d\tau} = c^2(\mathbf{x})\mathbf{p} \quad (5.3.1)$$

$$\frac{d\mathbf{p}}{d\tau} = -\frac{1}{c(\mathbf{x})}\nabla c(\mathbf{x})$$

where $\mathbf{x}(x_1, x_2, x_3)$ represents any position in the subsurface, $c(\mathbf{x})$ is velocity, τ refers to travel time, \mathbf{p} is slowness vector denoted as

$$\mathbf{p}(\mathbf{x}) = \nabla\tau(\mathbf{x}) = \frac{1}{c(\mathbf{x})}(\vec{i} \sin \phi \cos \theta + \vec{j} \sin \phi \sin \theta + \vec{k} \cos \phi)$$

for $0 \leq \theta \leq 2\pi$, $0 \leq \phi \leq \pi$

where ϕ, θ are the angle of the ray at point \mathbf{x} , and $\vec{i}, \vec{j}, \vec{k}$ are direction units.

For small steps (in time or space), the ray can be thought as a straight line. Then, after some manipulations, the equation (5.3.1) can be rewritten as

$$\begin{aligned} \frac{dx_1}{dt} &= c(\mathbf{x}) \sin \theta \\ \frac{dx_2}{dt} &= c(\mathbf{x}) \cos \theta && \text{for 2D,} \\ \frac{d\theta}{dt} &= -\frac{c(\mathbf{x})}{dx_1} \cos \theta + \frac{c(\mathbf{x})}{dx_2} \sin \theta \end{aligned} \quad (5.3.2)$$

and,

$$\begin{aligned} \frac{dx_1}{dt} &= c(\mathbf{x}) \sin \phi \cos \theta \\ \frac{dx_2}{dt} &= c(\mathbf{x}) \sin \phi \sin \theta \\ \frac{dx_3}{dt} &= c(\mathbf{x}) \cos \phi && \text{for 3D.} \\ \frac{d\phi}{dt} &= \frac{c(\mathbf{x})}{dx_3} \sin \phi - \left[\frac{c(\mathbf{x})}{dx_1} \cos \theta + \frac{c(\mathbf{x})}{dx_2} \sin \theta \right] \cos \phi \\ \frac{d\theta}{dt} &= \frac{\frac{c(\mathbf{x})}{dx_1} \sin \theta - \frac{c(\mathbf{x})}{dx_2} \cos \theta}{\sin \phi} \end{aligned} \quad (5.3.3)$$

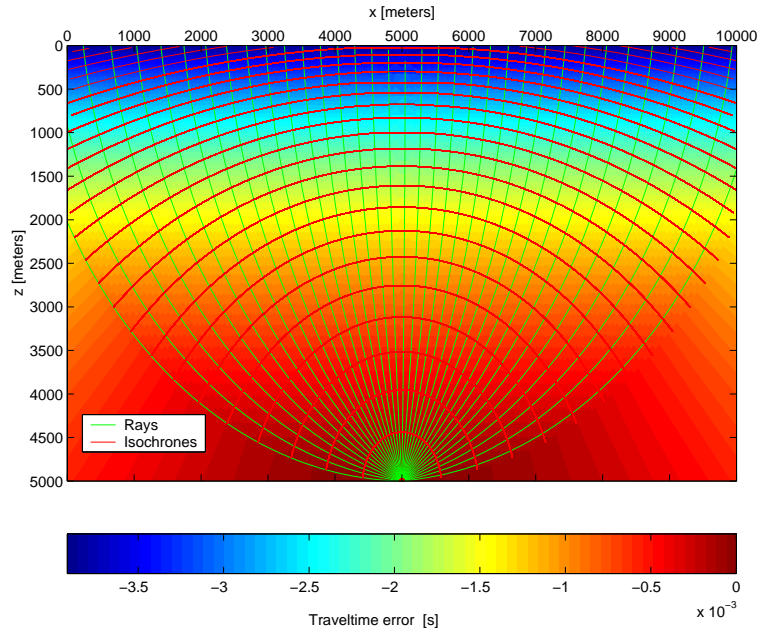


Figure 5.3: Comparing of analytic result with ray racing. Background is traveltime error(maximum error is less than 0.0039 seconds). The source is located at (5000m, 5000m).The wavefront is contoured in 0.080 seconds increments.

5.3.1 Accuracy of the travel times approximation

I have tested the accuracy of the method on two models. One is analytic gradient model with velocity $c = a + bz$ to test the travel time; another is a 16 layers model to test the angle and travel time. Both examples show high accuracy.

The gradient model has $a = 1000m/s$, and $b = 1.2s^{-1}$. I shoot 179 rays from point (5000m, 5000m) with initial angle $-89 \sim 89$ using ray tracing and calculate the position of the wavefront at each $\Delta t = 4ms$, then calculate wavefront's travel time with analytic method. The range of the absolute error between two methods is less than 0.0039 seconds, see Figure 5.3.

For the 16 layers model, the analytical results (transmitted angles of the rays) are obtained by using Snell Law at each interface. I shoot 121 rays with angle $-60 \sim 60$. Figure 5.4 is the result I compare the results of the approximated ray tracing with the analytical results, Figure 5.5 is the relative traveltime error using

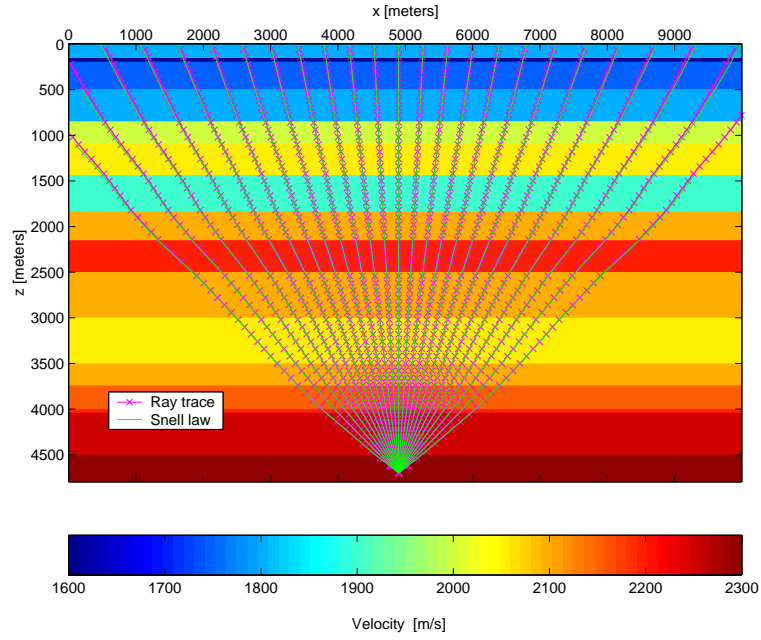


Figure 5.4: Comparing Snell Law model with ray racing. Background is layer velocity. The source is located at (4900m,4700m).

equation:

$$t_{error} = \frac{t_{ray} - t_{Snell}}{t_{Snell}}.$$

The analytic equation, given by (Vanelle, 2002), is

$$\tau = \frac{1}{b} \operatorname{arcosh} \left(1 + \frac{b^2 r^2}{2V_s V_g} \right),$$

where

$$\operatorname{arcosh}(y) = \log(y + \sqrt{y^2 - 1}),$$

where V_s, V_g are the velocities at source and receiver, r is the distance between source and receiver, b is the velocity gradient.

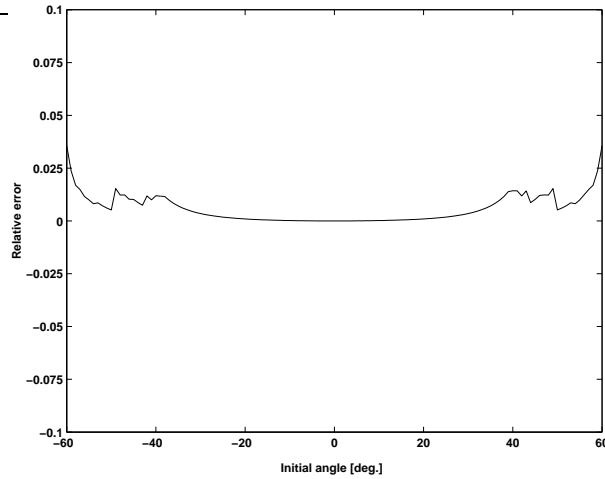


Figure 5.5: Relative traveltme errors that are computed with the Snell law model at the surface.

5.4 Geometrical spreading/amplitude approximation

Amplitude information is useful for migration and inversion. In order to obtain an approximate form of the amplitude, we begin with the amplitude in constant media

$$A = \frac{1}{R}, \quad (5.4.1)$$

where R is the distance between source and receiver (Figure 5.6A). In this figure, the length of arc l is

$$l = R\theta, \quad (5.4.2)$$

where θ is the angle between two rays. If the θ is small enough, the arc $l \approx d$. Then, substituting it to equation (5.4.2) and equation (5.4.1). Finally, we obtain

$$A = \frac{\theta}{d}, \quad (5.4.3)$$

In some sense, $\frac{\theta}{d}$ is the density of the rays. Therefore, we can use above equation to estimate amplitude. In 2D situation, the amplitude is

$$A = \sqrt{\frac{\theta}{d}}. \quad (5.4.4)$$

5.4. GEOMETRICAL SPREADING/AMPLITUDE APPROXIMATION

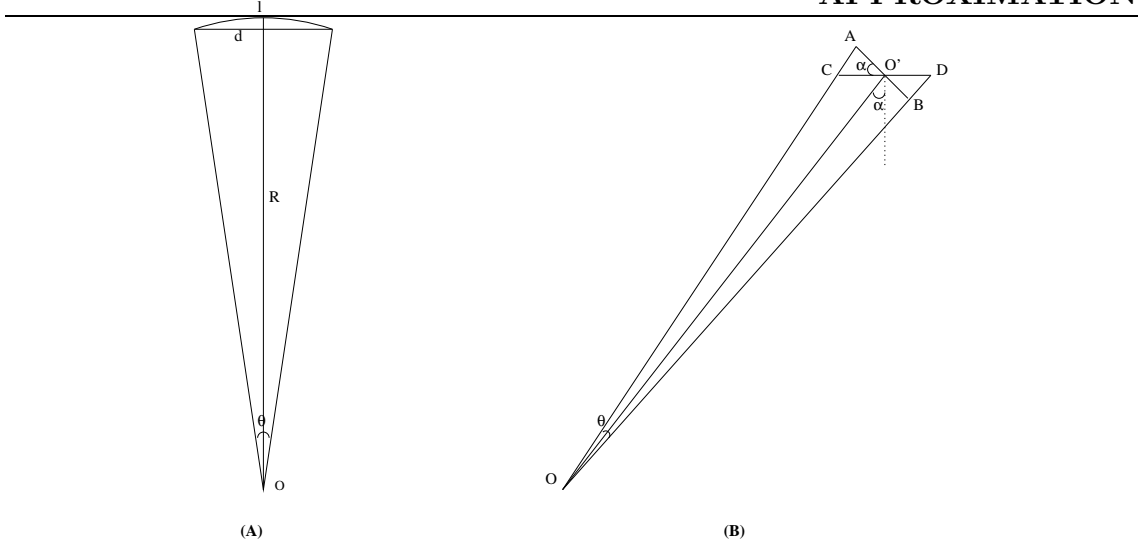


Figure 5.6: Amplitude in constant velocity media, initial angle is 0° (A), and any angle (B).

However, the above equations are only valid for the ray which is generated vertically to the surface, in other situations, a weight is needed. In Figure 5.6B, according to equation (5.4.3) the amplitude is $\frac{\theta}{AB}$. But we only know the length of CD . Therefore, an expression, which represents AB with CD , is needed. As mentioned above, the angle θ is small. Using simple geometric considerations we can obtain

$$\angle AO'C = \alpha, \quad OA \approx OO', \quad \angle OAO' \approx \angle OO'A = 90^\circ,$$

then we can derive

$$AO' = CO' \cos \alpha.$$

Because $AB = 2AO'$ and $CD = 2CO'$, after some manipulations, finally, we obtain

$$A = \sqrt{\frac{\theta}{d \cos \alpha}} \quad \text{for 2D.} \quad (5.4.5)$$

Usually, the rays reach the surface with almost right angle, therefore, equation (5.4.5) still can be simplified as equation (5.4.4).

5.4.1 Accuracy of the amplitude approximation

I first test the approximation for of the amplitude with a constant velocity model. In this case, the velocity is 3000 m/s. Source position is $x = 8000$ m, $z = 8000$ m. The 2D analytic equation I used here is

$$A = \frac{1}{\sqrt{r}}$$

where r is the distance between source and receiver. The compared results are shown in Figure 5.7.

I also test the approximated equation with a gradient model ($v = a + bz$). In this case, $a = 3000$ m/s, $b = 0.4$ s⁻¹. The source position is $x = 8000$ m, $z = 8000$ m. The analytic equation (Vanelle, 2002) I used here is

$$A = \sqrt{\frac{2}{\sqrt{b^2 r^4 + 4v_s v_g r^2}}}$$

where v_s, v_g are the velocities at source and receiver, r is the distance between source and receiver, b is the velocity gradient. Figure 5.7, Figure 5.8 and Figure 5.9 show the comparing result. The relative errors are negligible, even for very large velocity perturbation.

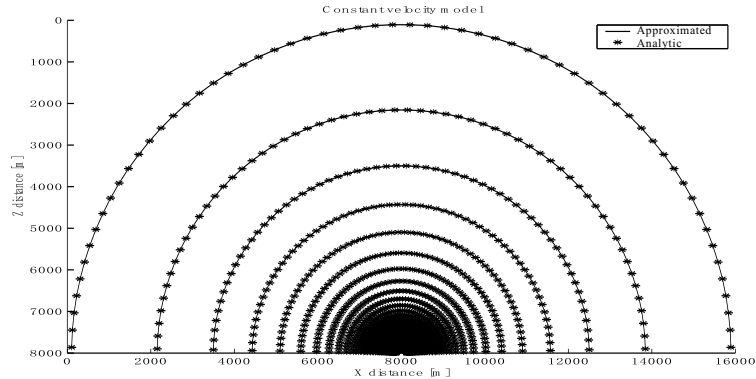


Figure 5.7: Comparing amplitude between analytic method and approximate method using constant velocity model. The source is located at (8000 m, 8000m). The amplitude contour increment is 0.1.

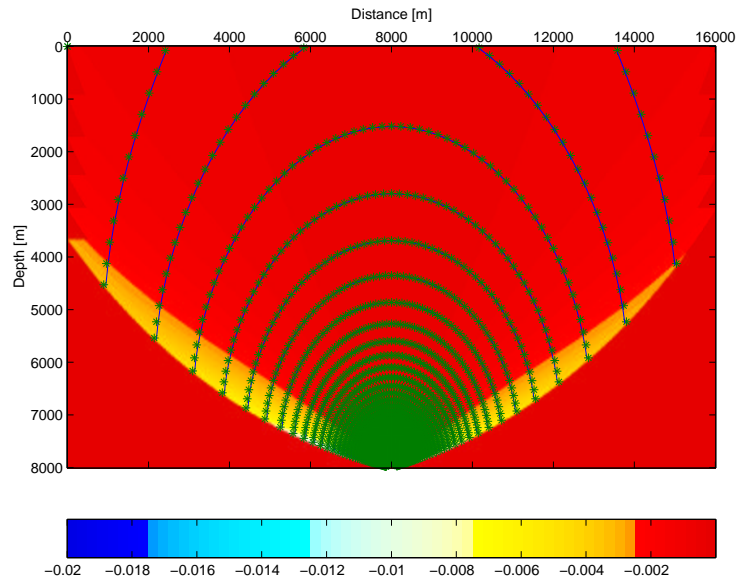


Figure 5.8: Comparing amplitude between analytic method and approximate method using gradient velocity model ($v = 3000 + 0.4z$). The source is located at (8000 m, 8000m). The amplitude contour increment is 0.1.

5.5 Summary

Since an efficient strategy for calculating the Green's functions with high accuracy will significantly reduce the amplitude-preserving migration cost, I propose an approximation to the amplitude of the Green's function for the weighted pre-stack Kirchhoff migration based on the eikonal equation.

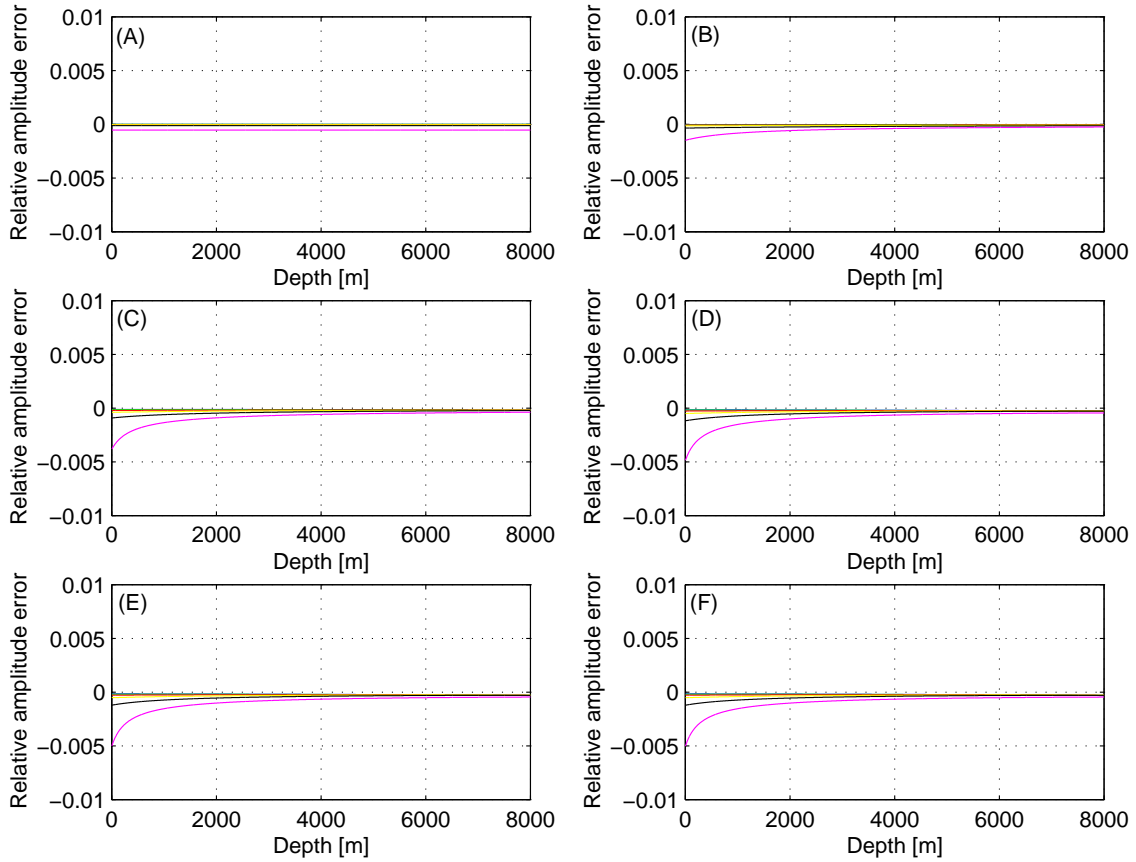


Figure 5.9: Relative amplitude error between analytic method and approximate method using gradient velocity model $v = a + b.z$ [m/s]. The source is located at (8000 m, 8000 m). $a = 3000$ and $b = 0$ (A), 0.1 (B), 1 (C), 10 (D), 100 (E), and 1000 (F). The initial angle is 0° (blue), 15° (green), 30° (red), 45° (yellow), 60° (black), 75° (magenta). Note that the relative error is small (less than 0.5%).

Chapter 6

Synthetic and field data examples

6.1 Introduction

In the previous chapters, the discrete inverse theory was reviewed. The proposed algorithm for AVA and rock properties inversion was presented as well. The goal now is to exhibit with examples the performance of the proposed algorithm. Since it is difficult to test the accuracy of a method for an unknown real earth, the method will be applied to a simplified earth model (synthetic data).

As part of the accuracy test, modeling (or generating) a synthetic data set is an important step. Generally, in order to validate an inverse method, the synthetic data should be both as exact and as detailed as one wants (Gray et al., 2001). Also, the modeling method for the synthetic data should be different from the one that the proposed inverse method is based on (Kuehl, 2002). On the whole, the forward modeling must be a different, and more accurate operator.

Since full wave equation finite difference (FD) modeling has no aperture limitations, and generates all the events along with the wave equation (i.e., multiples and direct waves), therefore, instead of using approximate high frequency asymptotic method from which the inverse operators are derived (section 2.1), the FD method is an ideal way to obtain the synthetic data.

Because of the difficulties of modeling real earth data with the FD techniques, traditionally, the earth model, from which the synthetic data is generated, is simplified and idealized from the real earth. For example, a 3D elastic earth is simplified

as a 2D, or 2.5D (Bleistein, 1986) acoustic model, such simplification may exist in some definite situations. For example, as seismic data are collected along straight lines. The third dimension can be omitted. Thus, the data sets are two dimensional, and 2.5D assumption compensates the amplitude loss due to 2D assumption. If the P wave propagation governs in the entire volume, P waves propagating in elastic earth can be approximated by an acoustic wave model.

6.2 Synthetic data examples

Synthetic data tests are essential to calibrate an inverse method. This is because the details of the earth model is known before the inversion. Comparing the inverted result with the known image, the synthetic examples will illustrate advantage and pitfall of a method. Moreover, such applications can update the algorithm by fine-tuning the inverse code.

6.2.1 Seismic modeling for synthetic data test

I have been studying the problem of retrieving angle gathers for reflectivity inversion, as well as the problem of recovering rock properties in the previous chapters. As part of my research, I now have to generate a synthetic data set. The latter is used to test the accuracy of the rock properties inversion and angle gather migration/inversion code that I have been developing as part of my thesis research. Due to the difficulties of modeling three dimensional elastic data with a FD technique, the synthetic data are generated in two dimensional isotropic acoustic models. Once I have set up a synthetic "Earth Model", this is the distribution of velocities and densities in a 2D grid, I use acoustic FD to synthesize seismic data. For this purpose, I use the acoustic FD code provided by the Seismic Unix (`sufdmod2`). Such method is an approximation to the wave equation, but it is more accurate than the Kirchhoff integrals.

6.2.2 Inverse algorithm for 2D acoustic synthetic data

After computing the synthetic data, the perturbation of rock properties are recovered by using the proposed algorithm which is composed of the Kirchhoff migration/inversion and A&R inversion algorithm. The Kirchhoff algorithm, integrated with A&R inversion algorithm, is capable of performing both the well known Kirchhoff sum for migration (this is the so called adjoint operator) and the forward modeling Kirchhoff operator. In other words, the algorithm can generate outputs from operators \mathbf{G} (forward) and \mathbf{G}^T (adjoint).

Since the synthetic data is generated from a 2D acoustic model, the operator which I present in chapter 4 must be changed from a 3D elastic case to the 2D acoustic one. To be more precise

$$\mathbf{G}[f(\mathbf{x})] = \mathcal{K}\mathcal{Z}[f(\mathbf{x})] = \mathcal{C}\mathcal{L}\mathcal{Z}[f(\mathbf{x})] \quad (6.2.1)$$

where 2D Kirchhoff operator \mathcal{K} denotes

$$u_S(\mathbf{r}, \mathbf{s}, \omega) = |\omega| \int_S R(\mathbf{x}, \theta) A(\mathbf{r}, \mathbf{x}, \mathbf{s}) \left| \frac{2 \cos \theta}{c(\mathbf{x})} \right| e^{i\omega\tau(\mathbf{r}, \mathbf{x}, \mathbf{s})} W(\omega) d^2\mathbf{x}, \quad (6.2.2)$$

with $A(\mathbf{r}, \mathbf{x}, \mathbf{s})e^{i\omega\tau(\mathbf{r}, \mathbf{x}, \mathbf{s})}$ being the 2D Green's function, and the 2D A&R operator denotes

$$R(\mathbf{x}, \theta) = \mathcal{Z}[f(\mathbf{x})] = \frac{1}{2}(1 - \sin^2 \theta) \frac{\Delta\rho}{\rho} + \frac{\sec^2 \theta}{2} \frac{\Delta v_p}{v_p}. \quad (6.2.3)$$

This equation expresses a relationship between the amplitude in the CIGs and the physical parameters that could be associated to rock properties. In seismic exploration, we cannot neglect the contribution from v_s . In such case, full A&R approximation is needed. It does not make sense of inverting rock properties without including v_s . It is only for synthetics constructed with the acoustic wave equation that v_s is not taken into account in the inversion.

Given the forward/adjoint operators, the 2D inversion can be realized by using the algorithm presented on section 4.4.

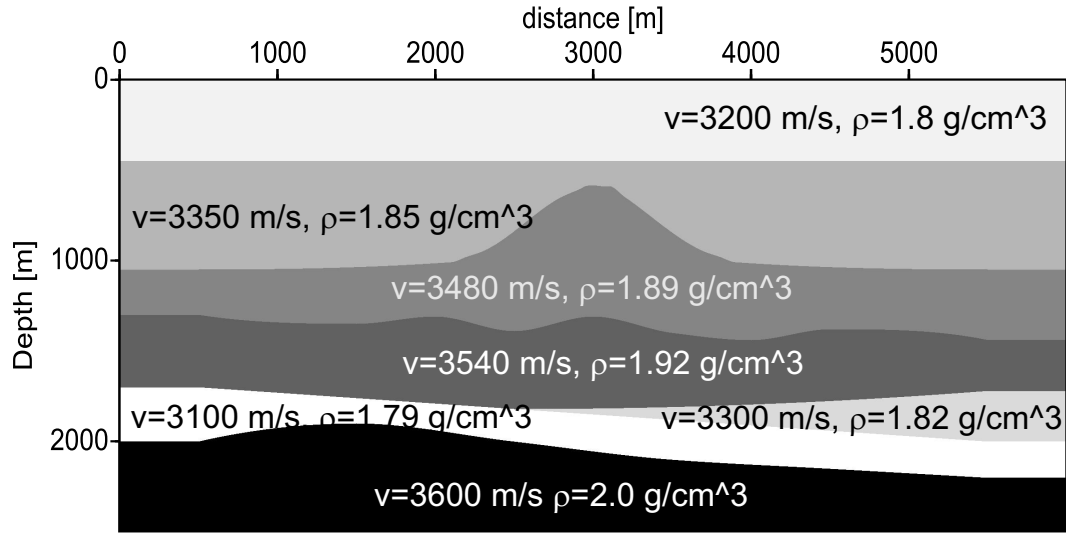


Figure 6.1: Model with structure.

Number of shots	Shot spacing [m]	First shot position (x, z) [m]	Number of receivers per shot	Receiver spacing [m]	First receiver offset [m]
51	20	(2000, 0)	201	20	2000

Table 6.1: Acquisition geometry for synthetic model.

6.2.3 Simple model with structures

The model has seven layers, including a horizontal layer, a fold, a pinch out and interfaces with topography (Figure 6.1). This acoustic model parameters are expressed as compressional velocities and densities, ranging from 3100 m/s to 3600 m/s, and from 1.79 g/cm³ to 2.0 g/cm³, respectively. In order to validate the high frequency assumption, the maximum relative perturbations of velocity and density are chosen less than 15% at the interfaces.

To generate the acoustic data using FD, I have adopted a source function with central frequency $f_c = 30$ Hz. The sampling interval and grid sampling are com-

puted to honor stability conditions¹. The velocity and density model extend from $x = 0$ to $x = 6000$ m and $z = 0$ to $z = 2500$ m, with grid intervals $\Delta x = 2.5$ m and $\Delta z = 2.5$ m. The sampling rate of data is $\Delta t = 4$ ms. The details of acquisition geometry for the experiment are specified in Table 6.1. Given above parameters, the data are generated by the acoustic FD code provided by Seismic Unix (`sufdmod2`). Figure 6.2 shows one shot gather of the synthetic data. The shot position locates at $x = 2040$ m, and $z = 0$ m (or No. 101 trace). The reflection waves exhibit clearly amplitude variation versus offset (AVO)².

The first arrivals, which are not needed for reflection data image, are muted from the data. Beside of the head waves, there are other noises (i.e., multiples and edge diffraction waves). Since those noises are weak comparing to the primary reflections, I leave them on the data to test the proposed algorithm under more difficult situations. In addition to the noise problem, the wavelet, which is used by the FD code of Seismic Unix, will bring some time delay³. The total delay is half length of the period of the wavelet— $\frac{T}{2}$.

Green's function

As mentioned before, the Green's function should be calculated before the Kirchhoff migration/inversion on a macro velocity model. The macro velocity is obtained from the earth model using a low pass filter. The smoothed macro velocity model is showed in Figure 6.3.

Based on the algorithm described in section 4.4, the rock properties and CIGs are obtained. The detail steps are

1. Calculate the Green's function table with target oriented ray tracing method on the migration velocity model. I shoot 121 rays at each subsurface grid point

¹The condition for stability is $\frac{v_{max}\Delta t}{\Delta x} \leq \frac{2}{\sqrt{a}}$, with constant a being the sum of the absolute value of the weight for the various wavefield terms in the finite-difference approximation for ∇^2 . Details about the stable condition, please see Lines et al. (1999).

²For example, the first event of Figure 6.2B becomes more and more clear along with the offset increasing.

³The time delay is caused by convolving a non-zero phase wavelet with the reflectivity series.

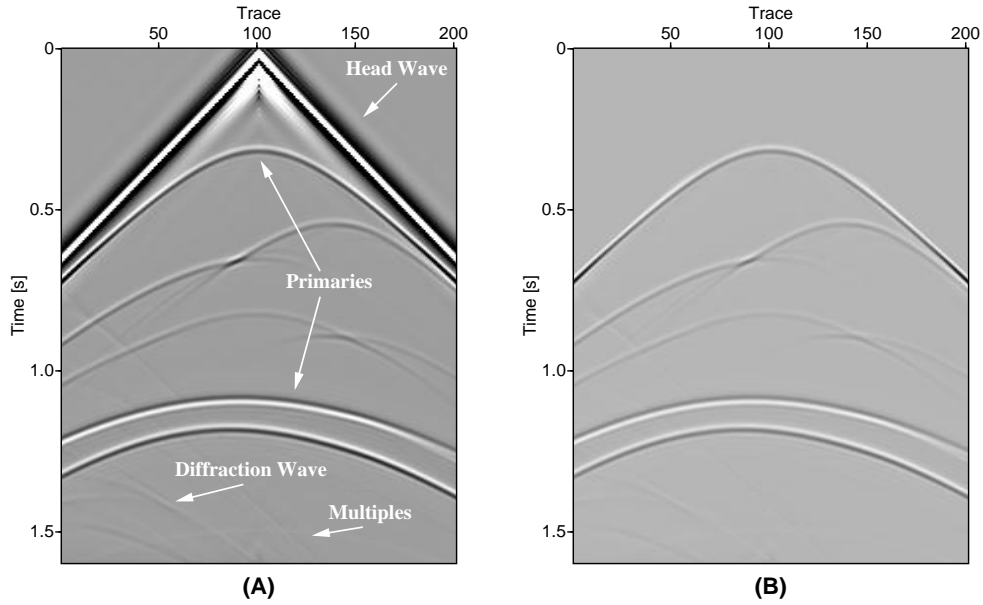


Figure 6.2: One common shot gather of synthetic data before (A), and after (B) muting the head waves. Shot position is (2040 m, 0 m).

in the range of $-80^\circ \sim 80^\circ$, with 1° interval. The computed Green's function table is stored in file for next step use.

2. Initialize the model parameters $(\frac{\Delta\rho}{\rho}, \frac{\Delta v_p}{v_p})$ with zero vector. The maximum iteration is set to 20, and the tolerance is set to $e_{max} = 10^{-7}$.
3. Try different sets of tradeoff parameters. Each time, I set the $\lambda = \mu$ which means giving the same weight to smoothness and sparseness. I totally try three sets of the tradeoff parameters, $\lambda = \mu = 0.1$, $\lambda = \mu = 0.01$, and $\lambda = \mu = 0.005$.
4. Input the other parameters for the algorithm, such as the data, the Green's function table and the migration velocity model etc., then run the CG code.
5. Visualize the result, such as stacked imaging, inverted model parameters $(\frac{\Delta\rho}{\rho}, \frac{\Delta v_p}{v_p})$ and check difference between the reconstructed synthetic data with original data, then choose the best one. For this simple model, I select the tradeoff

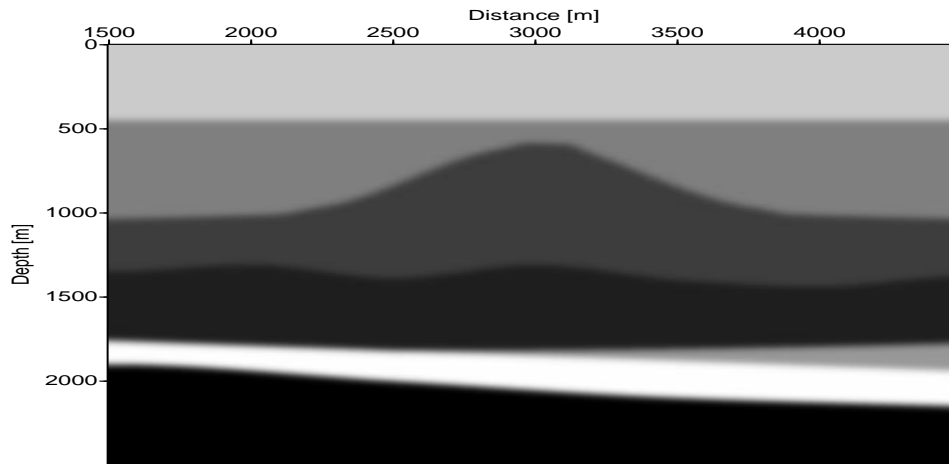


Figure 6.3: Macro velocity model obtained by using a low pass 2D filter.

parameters $\lambda = \mu = 0.01$.

The accuracy of the method is determined by comparing the inverted result with the true model, such as stacked image, AVA curves and rock parameters, etc.

Stacked image

The goal of the stack is to lineate the subsurface structures. Therefore, stacking the inverted result can examine the structural imaging capabilities of the inverse operators. Stacking is the processing that sums the CIGs along a parameter (i.e., offset, angle). Since such processing can enhance the ratio of signal-to-noise and suppress imaging artifacts and multiples, traditionally, it is used as a standard step in seismic data process to improve the image quality.

The results prove that the Kirchhoff propagator is accurate to recover a good image of the synthetic model (Figure 6.4). However, the inverted image is not spiky, which means the proposed algorithm does not recover the partially lost frequency information caused by band pass wavelet.

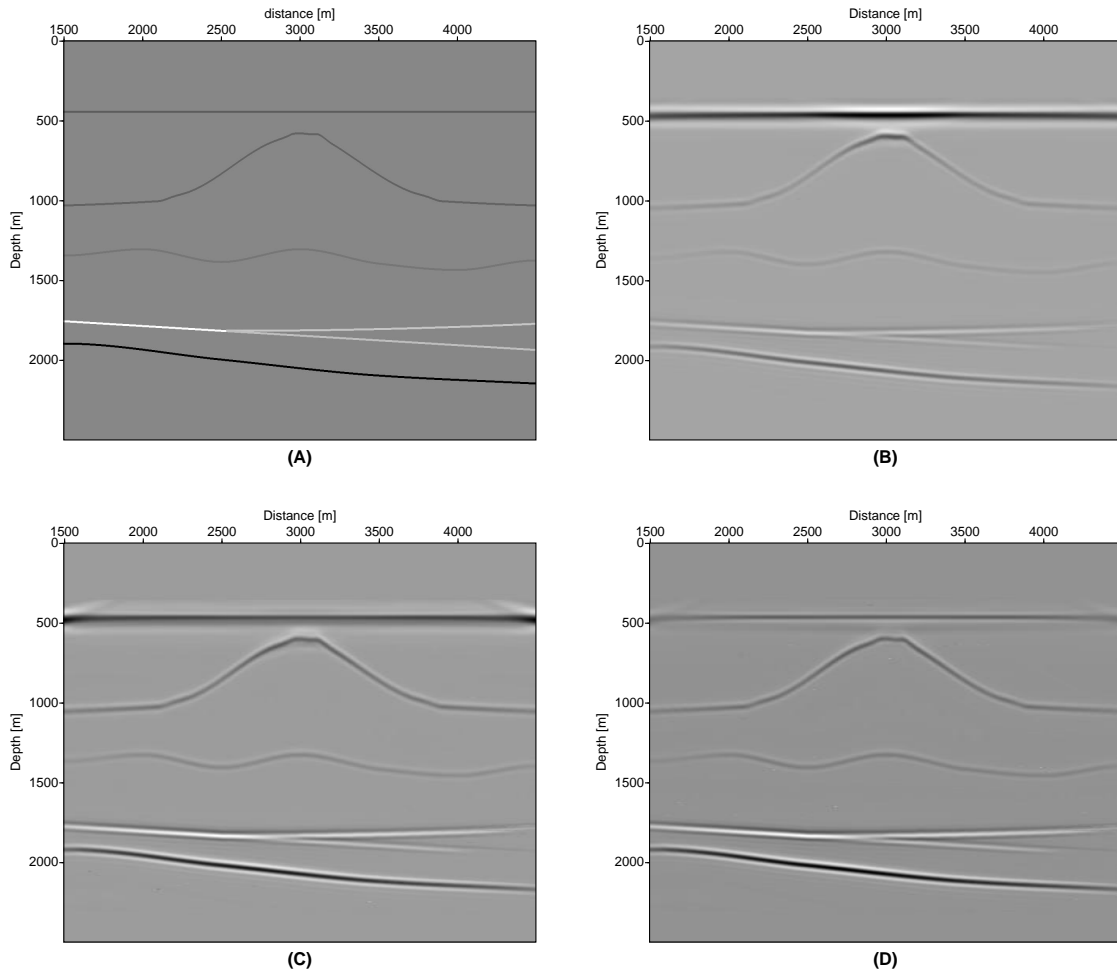


Figure 6.4: Comparison the structure of the inverted image with the true model. (A) True image. (B) Stacked image. (C) Inverted perturbation of v_p . (D) Inverted perturbation of ρ . Note that the recovered image is not spiky due to the band-limited wavelet.

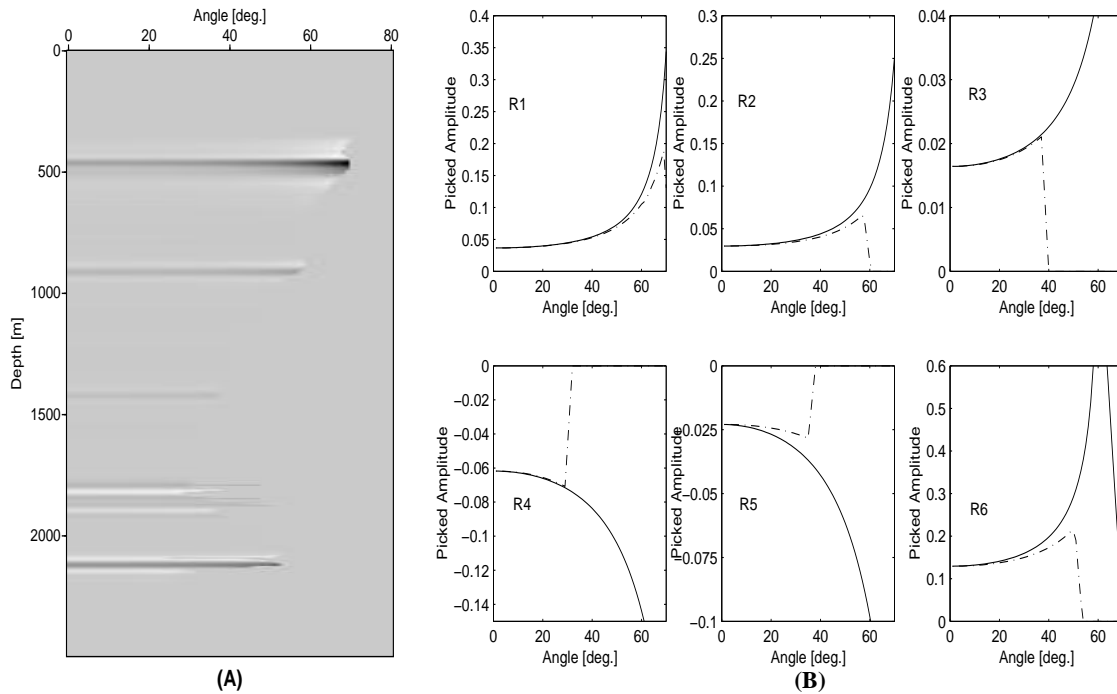


Figure 6.5: Inverted CIGs (A) and corresponding AVA (B) for synthetic data at $x = 3600$ m. The labels R1-R6 correspond to the six reflectors from top to bottom. All picked values (dot-dash lines) have been scaled with the true AVA (solid lines). Note that all of the AVA of the reflectors drop down to the zero at high angles due to the limit aperture effects.

CIGs and AVA analysis

Retrieving correct the structural information is only a prerequisite for a successful inversion. The more challenge part is to obtain accurate amplitude information from CIGs and a good estimation of rock properties. As the CIGs describe the amplitude variation along the reflection angle for a series of positions. Thus, the events on the CIGs must be flat. Furthermore, the amplitude variation of any position should fit the true AVA. Because the synthetic data are generated by using acoustic wave equation, the inverted AVA curve should fit the acoustic AVA equation. Such equation can be found in the book of Berkhout (1987).

$$R(\mathbf{x}, \theta_1) = \frac{\rho_2(\mathbf{x})v_2(\mathbf{x}) \cos \theta_1 - \rho_1(\mathbf{x})v_1(\mathbf{x}) \cos \theta_2}{\rho_2(\mathbf{x})v_2(\mathbf{x}) \cos \theta_1 + \rho_1(\mathbf{x})v_1(\mathbf{x}) \cos \theta_2}, \quad (6.2.4)$$

where \mathbf{x} is any position of subsurface, $\rho_1(\mathbf{x}), \rho_2(\mathbf{x})$, and $v_1(\mathbf{x}), v_2(\mathbf{x})$ represent the densities and velocities of the adjacent layers, respectively. The incident and transmitted angles denote θ_1, θ_2 respectively.

Under high frequency assumption, the above equation is a good approximation to the equation (6.2.3). Thus, the equation (6.2.4) can be used to test the inverted AVA.

Figure 6.5 depicts the inverted CIGs (A) and corresponding picked AVA (B) at position of $x = 3600$ m. R1-R6 corresponds the six layers from top to bottom in the CIGs. Due to the limited aperture effects, the CIGs is absent at large angle. Apart from those limited aperture effects, the CIGs is clean and free of alias. All events are flat along the horizontal direction and sparse along depth. The picked AVAs (dot-dash lines) also prove that the CIGs are in good agreement with the true AVA response. All curves fit the theoretical AVAs (solid lines) very well except the fourth layer.

Figure 6.6 illustrates the inverted perturbations of the velocity (A) and density (B) at $x = 2750$ m. The true perturbations are drawn with solid lines. The smeared results match the true variation closely. However, the error rises when the depth of layers increases. This is because no energy loss due to transmission is included in

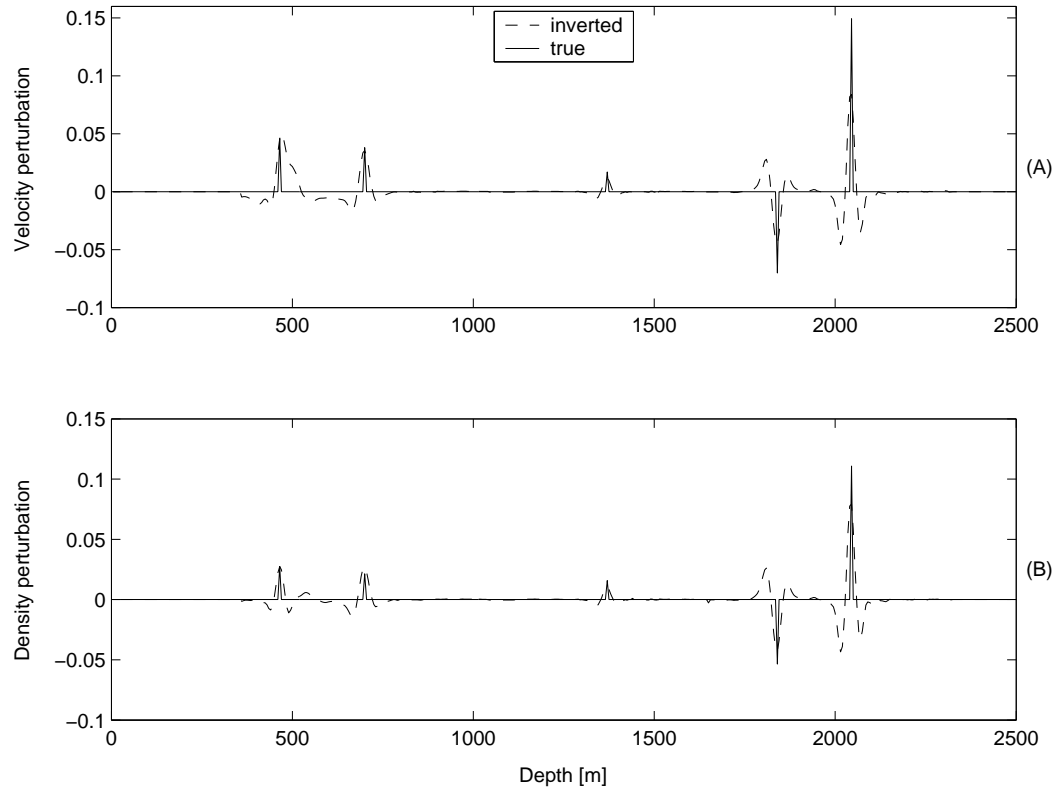


Figure 6.6: Inverted perturbations of velocity (A) and density (B) extracted from Figure 6.4C and Figure 6.4D respectively at $x=2750$ m. The inverted result (dash lines) have been scaled with the true variation (solid lines).

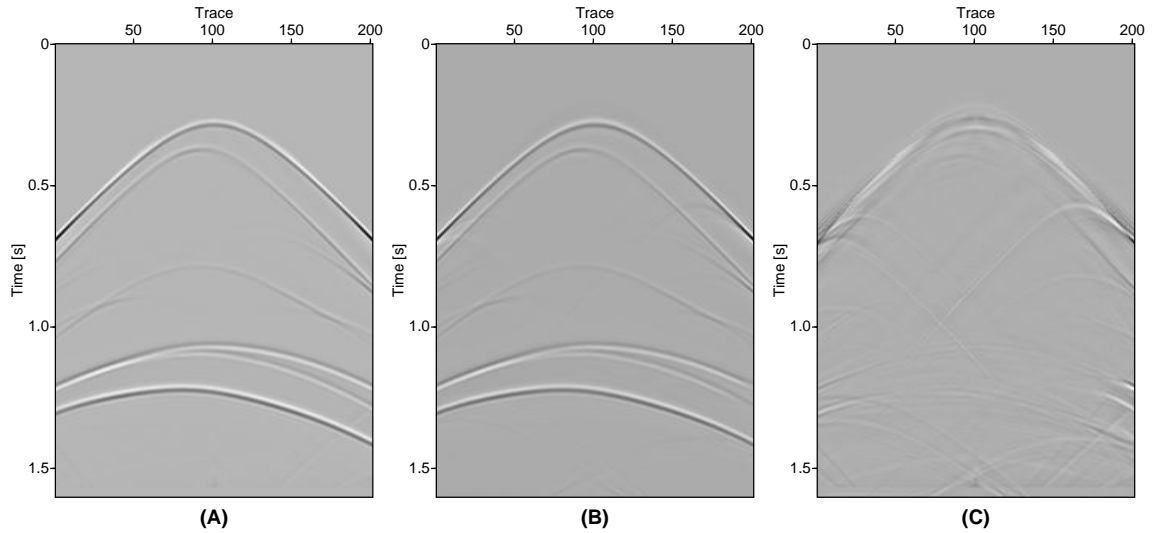


Figure 6.7: Comparison of original data (A) with reconstructed data (B) and the error (C) between them.

the inverse algorithm. Therefore, the accuracy of the inversion result degrades for deeper horizons.

The inverted results have been scaled with the true perturbations before plotting. The perturbation (or relative variation) for the velocity and the density in Figure 6.6 denotes as

$$\begin{aligned}\Delta\rho' &= \frac{\Delta\rho}{\rho} \quad \text{for density} \\ \Delta v' &= \frac{\Delta v}{v} \quad \text{for velocity}\end{aligned}$$

with $\Delta\rho$, and Δv being absolute variation of density and velocity of adjacent layers respectively, ρ , v being average of density and velocity of adjacent layers respectively.

Figure 6.7 exemplifies the error (C) between the original synthetic data (A) and the reconstructed data (B)⁴. The reconstructed data, which are generated by applying modeling operator to the inverted model, are consistent with the original synthetic data. Since the inverse algorithm is based on primary wave fields propaga-

⁴The errors (Figure 6.7 (C)) are amplified to the same magnitude before plotting.

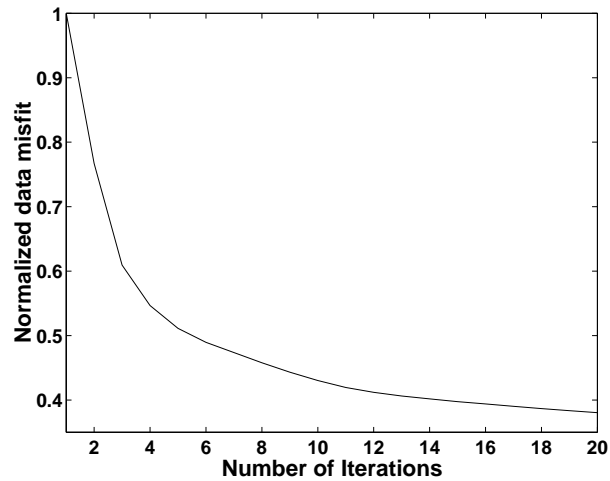


Figure 6.8: Normalized data misfit.

tion, the multiples and the edge diffraction waves were not taken into consideration. Therefore, the major error is caused by the energy of these two waves. Therefore, it is very important to de-multiple before the inversion.

Figure 6.8 shows the data misfit versus iteration. In this example, a total 20 iterations were needed to reach the solution that minimized the cost function of our inverse problem.

6.2.4 Marmousi model

The Marmousi (Versteeg and Grau, 1991) model is a complex structure model with numbers of very thin layers broken by several major faults and unconformity surface, which is based on a detailed geological 2D cross section of a real offshore Angola basin (Figure 6.9). The Marmousi data sets consist of 240 single-cable marine shot records which are acquired using acoustic finite-difference modeling. The sampling rate of data is $\Delta t = 4$ ms. The details of acquisition geometry for the experiment are specified in Table 6.2. Both velocity and density are various. This model was generated by the French Petroleum Institute, and was released to the industry for the purpose of testing migration and velocity estimation techniques (Versteeg, 1994).

The inverse steps are the same as the simple model:

Number of shots	Shot spacing [m]	First shot position (x, z) [m]	Number of receivers per shot	Receiver spacing [m]	First receiver offset [m]	Receiver depth [m]
240	25	(3000, 8)	96	25	200	12

Table 6.2: Acquisition geometry for Marmousi model.

1. The Green's function table is calculate with target oriented ray tracing method on the migration velocity model. I shoot 242 rays at each subsurface grid point in the range of $-60^\circ \sim 60^\circ$, with 0.5° interval. The computed Green's function table is stored in a binary file for next processing step.
2. Initialize the model parameters $(\frac{\Delta\rho}{\rho}, \frac{\Delta v_p}{v_p})$ with zero values. The maximum iteration is set to 10, and the tolerance is set to $e_{max} = 10^{-7}$.
3. Try different sets of tradeoff parameters. I set the $\lambda = \mu$ which means giving the same weight to smoothness and sparseness. I totally try five sets of the tradeoff parameters, $\lambda = \mu = 0.5$, $\lambda = \mu = 0.1$, $\lambda = \mu = 0.05$, $\lambda = \mu = 0.01$, and $\lambda = \mu = 0.005$.
4. Input the other parameters for the algorithm, such as the data, the Green's function table and the migration velocity model etc., then run the CG code.
5. Visualize the result, such as stacked images, inverted model parameters $(\frac{\Delta\rho}{\rho}, \frac{\Delta v_p}{v_p})$ and check difference between the reconstructed synthetic data with original data, then I select the tradeoff parameters $\lambda = \mu = 0.1$.

Since the intricate structure of this model produces very realistic seismic data, the Marmousi model is an excellent test data set. However, many imaging methods cannot completely recover the target structure, while some methods can produce a nearly perfect image, but with more calculations. Thus, a compromise between the accuracy and efficiency should be the best way for industrial exploration. As mentioned earlier, the algorithm proposed in this thesis is based on the high frequency

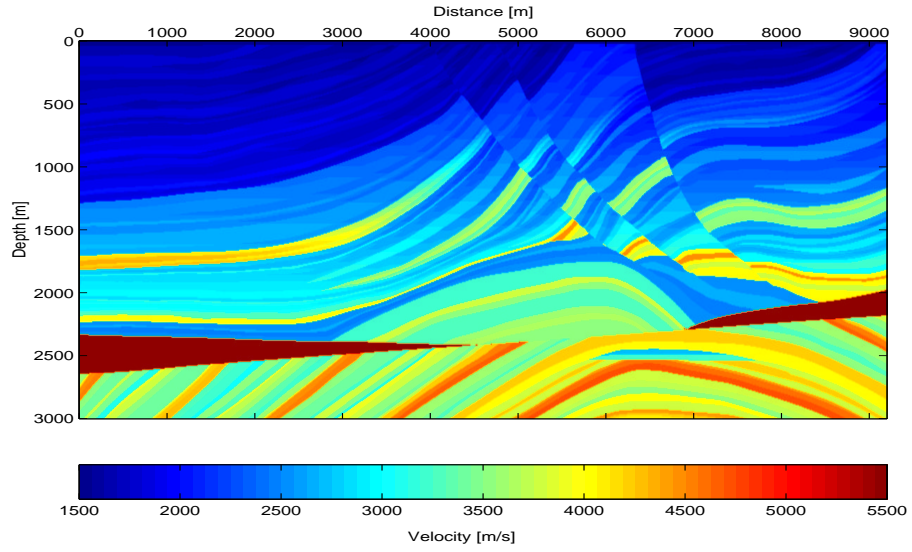
approximation. On the contrary, the condition of wave propagation in the Marmousi model is far from such approximation. Nevertheless, the proposed scheme proves to produce a good structural image of the Marmousi model. Figure 6.10 depicts a good result of the inverted stack image (A) of the Marmousi model. The retrieved perturbations of the velocity (B) and density (C) are also showed together. Despite of the dim effects, the faults and oil trap can still be seen clearly. This proves that the inverse algorithm is accurate enough to recover the structure of the 2D complex model.

Now, the focus is on retrieving rock properties and AVA analysis. At this stage, those inverse steps are still challengeable for highly complex earth models. Since amplitude recovering is more vulnerable to operator accuracy than structural imaging, it is crucial to select the areas for AVA where the process will be successful. The criteria for such selection, as presenting in Kuehl (2002) thesis, are:

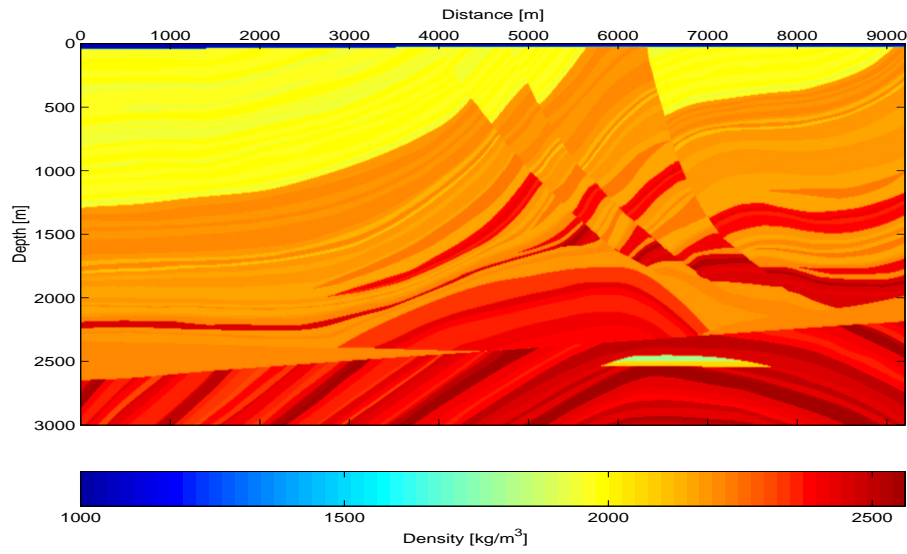
1. the depth points should be located in the upper half of the model so as to ensure sufficiently large angle range coverage.
2. ... the picked reflection event, the target, ought to be generated by a single, local plane, interface.

Obviously, only a few of the reflections of the Marmousi model satisfy the above criteria. Figure 6.11 shows the CIGs and corresponding picked amplitudes. Figure 6.12 and Figure 6.13 illustrate the inverted perturbations of the velocity (A) and density (B) at $x = 3600$ m (less complex structure zone) and $x = 6425$ m (complex structure zone). The true perturbations are drawn with solid lines. The smeared results match the true variation closely above the depth $z = 1500$ m. Due to the multiples and transmission losses, the error increases with depth.

Figure 6.14 exemplifies the error (C) between the original synthetic data (A) and the reconstructed data (B) for one shot gather. The reconstructed data are consistent with the original synthetic data except for the deep events.



(A)



(B)

Figure 6.9: Compressional velocity field (A) and density field (B) of Marmousi model.

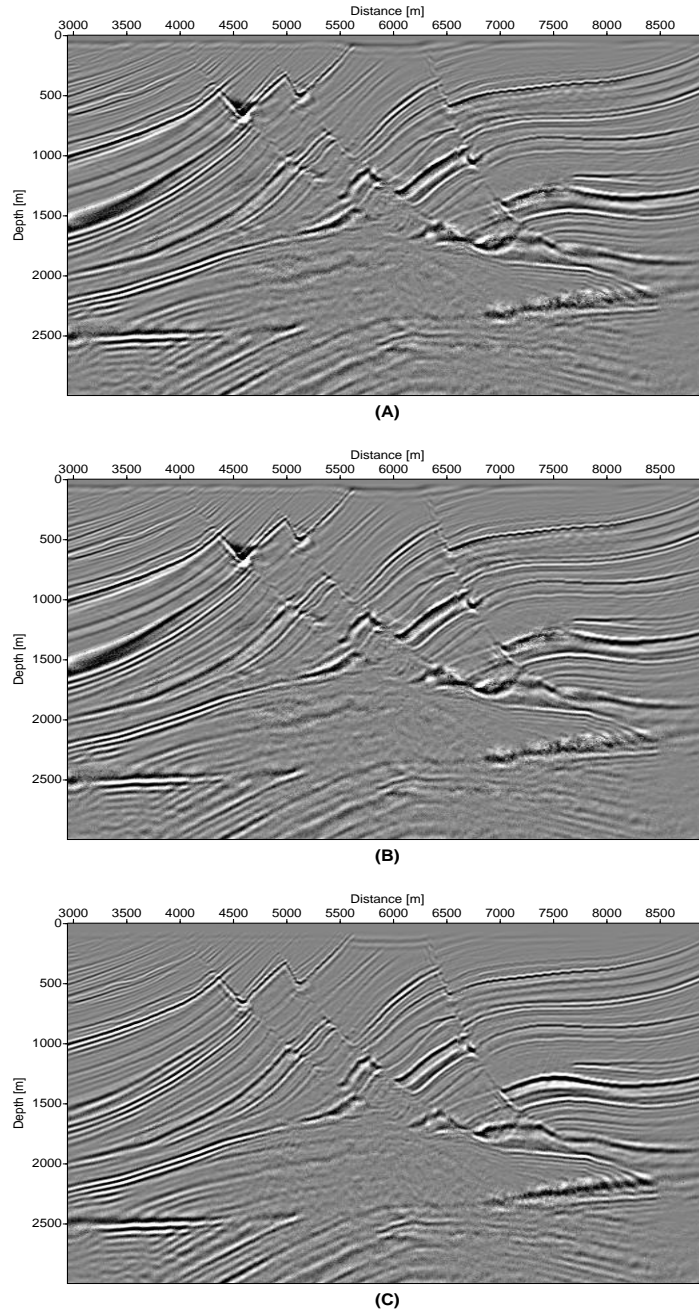


Figure 6.10: Inverted stack image (A), variation of velocity (B) and density (C) of the Marmousi model.

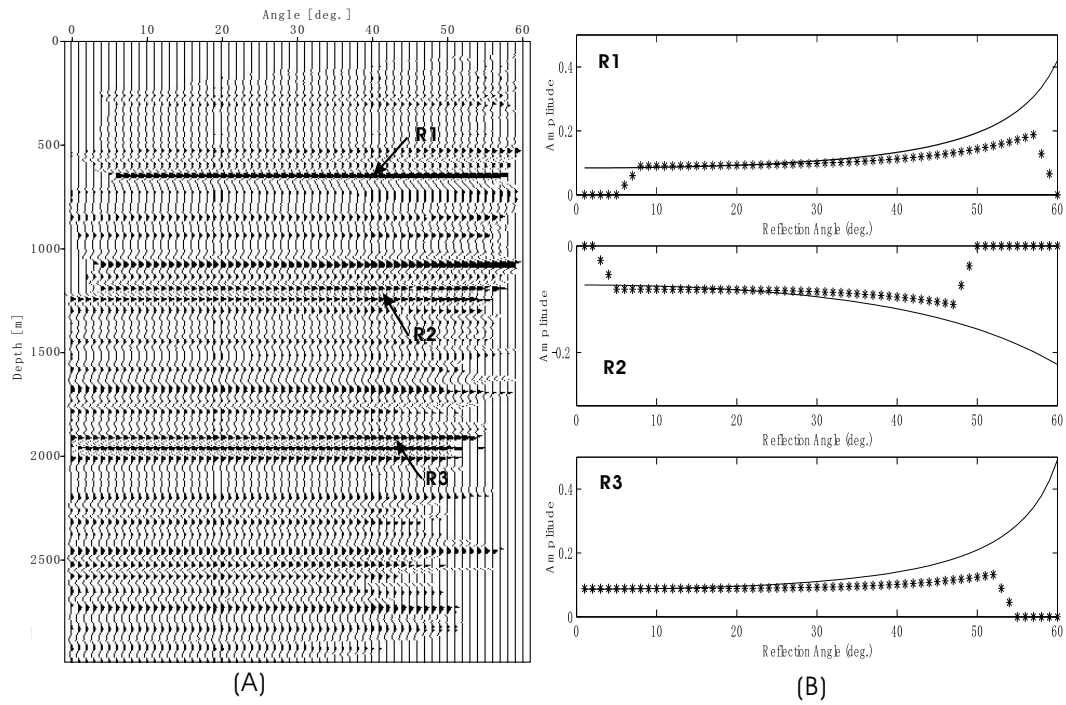


Figure 6.11: Inverted CIGs (A) and corresponding AVA (B) for Marmousi data at $x = 6400$ m. The labels R1-R3 correspond to the three reflectors from top to bottom. All picked values (dot-dash lines) have been scaled with the true AVA (solid lines). Note that all of the AVA of the reflectors drop down to the zero at low or/and high angles due to the limited aperture effects.

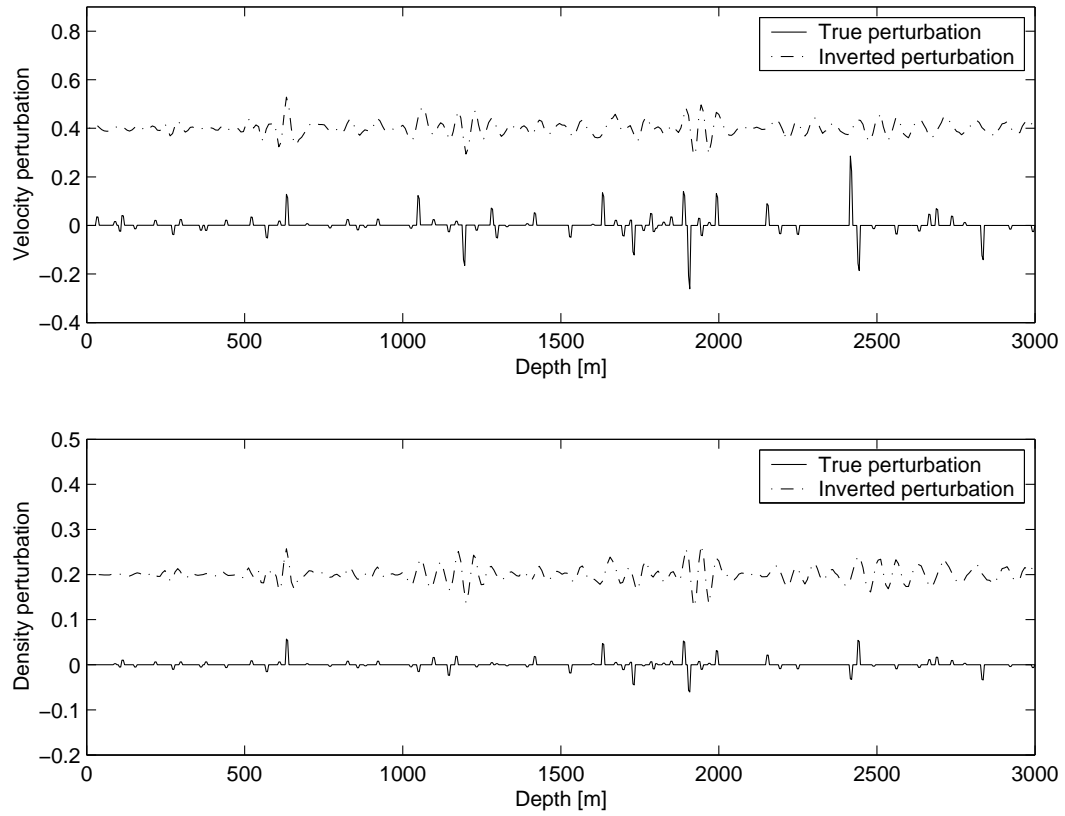


Figure 6.12: Inverted perturbations of velocity (A) and density (B) extracted from Figure 6.10B and Figure 6.10C respectively at $x = 3600$ m. The inverted results (dash lines) have been scaled with the true variation (solid lines).

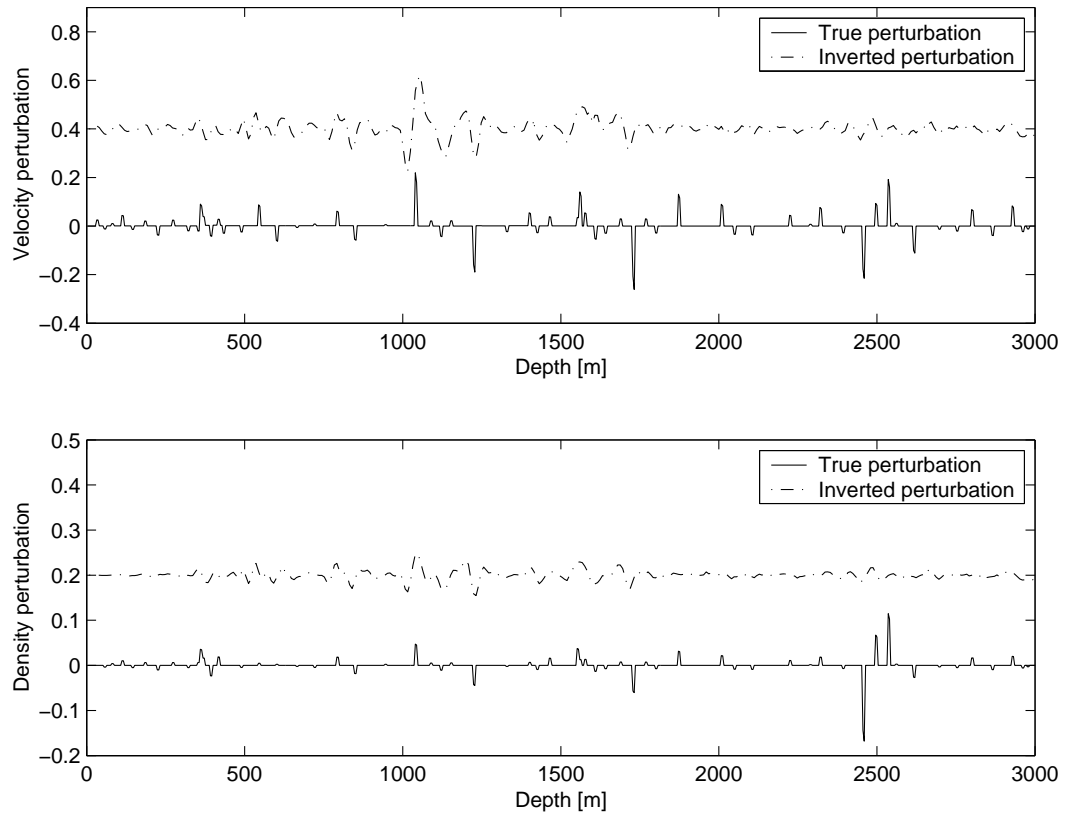


Figure 6.13: Inverted perturbations of velocity (A) and density (B) extracted from Figure 6.10B and Figure 6.10C respectively at $x = 6425$ m. The inverted results (dash lines) have been scaled with the true variation (solid lines). Note that the transmission loss debases the inverted result for deeper layers.

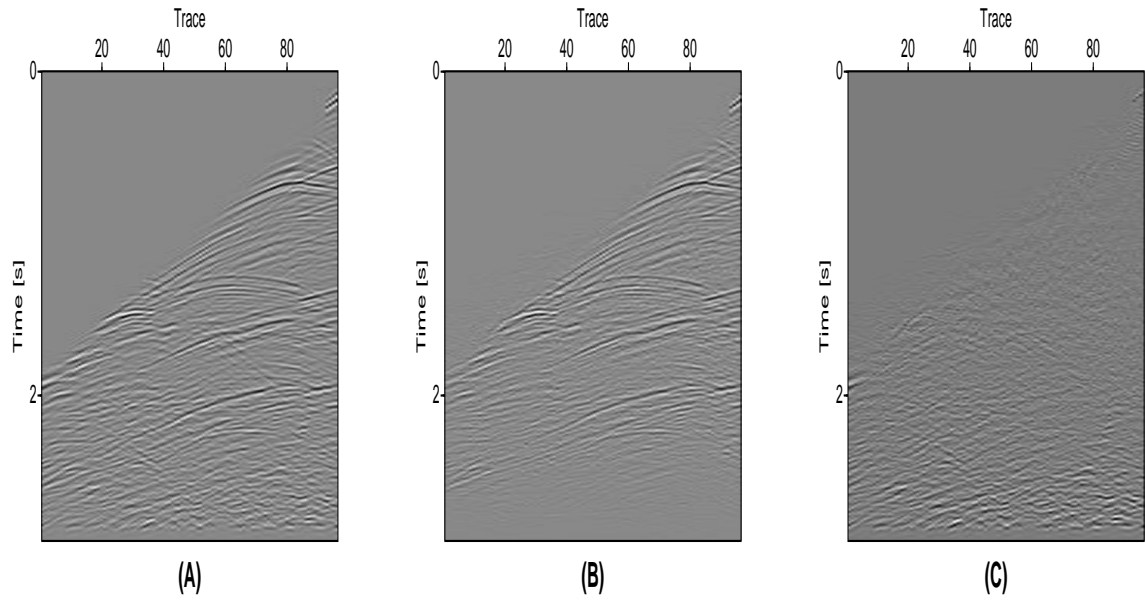


Figure 6.14: Comparison of Marmousi data (A) with reconstructed data (B) and the error (C) between them.

6.3 Real data example

The algorithm now is applied to a real data. The data have been acquired in the Gulf of Mexico by Western Geophysical and donated to academic and industrial research groups for test purposes. The Gulf of Mexico data sets are collected along a relatively deep sea (1400 m below sea level). The start time is $t = 1.5$ s and the sampling rate of data is $\Delta t = 4$ ms. The details of acquisition geometry are specified in Table 6.3. Only a small part of the data have been used to test our algorithm (first 100 shorts) (Figure 6.15). The following procedures are applied to the data to do the inversion:

1. Compute Green's function tables based on the velocity model provided by (Figure 6.16). The velocity model is computed using Dix inversion. I shoot 121 rays at each subsurface grid point in the range of $-60^\circ \sim 60^\circ$, with 1° interval. The computed Green's function table is stored in a binary file for the next step.
2. Initialize the model parameters $(\frac{\Delta\rho}{\rho}, \frac{\Delta v_p}{v_p}, \frac{\Delta v_s}{v_s})$. The maximum iteration is set to 10, and the tolerance is set to $e_{max} = 10^{-7}$.
3. Try different sets of tradeoff parameters. I set the $\lambda = \mu$ which means giving the same weight to smoothness and sparseness. I totally try three sets of the tradeoff parameters, $\lambda = \mu = 0.1$, $\lambda = \mu = 0.01$, and $\lambda = \mu = 0.005$.
4. Input the other parameters for the algorithm, such as the data, the Green's function table and the migration velocity model etc., then run the CG code.
5. Visualize the result, such as stacked images inverted model parameters $(\frac{\Delta\rho}{\rho}, \frac{\Delta v_p}{v_p}, \frac{\Delta v_s}{v_s})$ and check difference between the reconstructed synthetic data with original data. In this example I selected the tradeoff parameters $\lambda = \mu = 0.005$.

The inverted perturbations of P-wave, S-wave velocity and density are shown in Figure 6.17. The signal to noise (S/N) ratio and stability of the inversion is good

Number of shots	Shot spacing [m]	Number of receivers per shot	Receiver spacing [m]	nearest offset [m]	farthest offset [m]
2000 – 3000	26.7	180	26.7	20.6	4876

Table 6.3: Acquisition geometry for Gulf of Mexico data set.

for P wave velocity and density perturbations, and medium for S wave velocity perturbation. The CIGs at $CMP = 1069$ is shown in Figure 6.18. Unfortunately, there is no borehole in the area. The inverted result can not be validated by further information.

6.4 Summary

In this chapter, the integrated method was successfully applied to invert the rock properties from synthetic data and real data. The proposed algorithm appears robust and efficient combining with target oriented ray tracing. Since CG inverse method performs both the forward and adjoint operators once in each iteration, the computational cost grows with the iteration number. Therefore, the Green's functions are calculated in advance and stored in computer memory to avoid extra calculations.

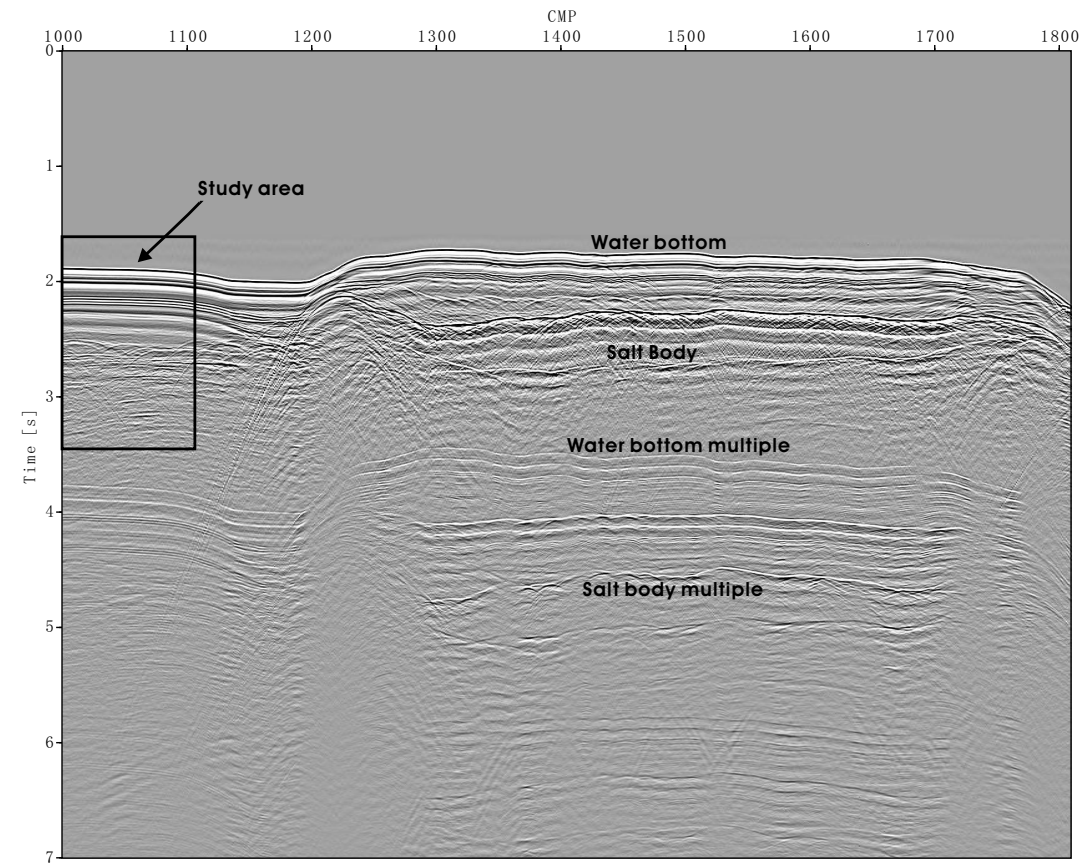


Figure 6.15: Near offset section with the study area.

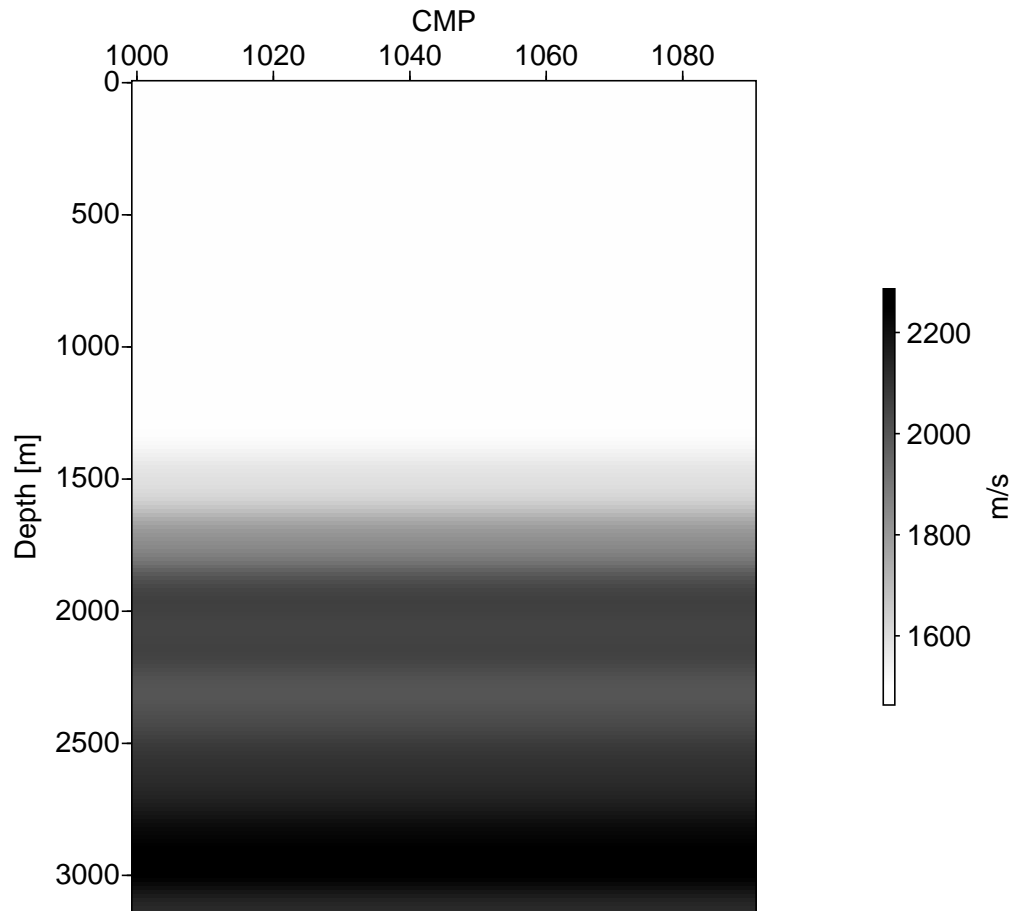


Figure 6.16: The macro velocity model for real data obtained by Dix inversion.

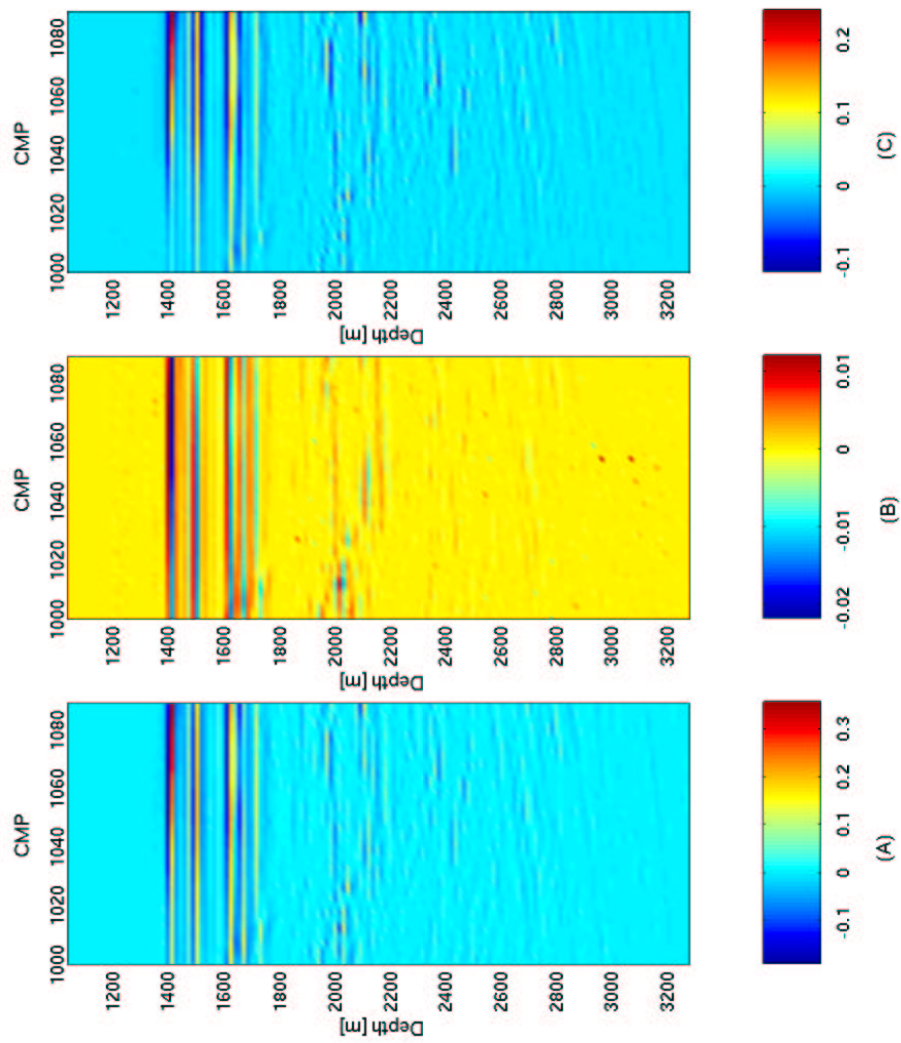


Figure 6.17: Inverted P-wave velocity perturbation (A), S-wave velocity perturbation (B), and density perturbation (C) for real data. The original value is multiplied by 2000.

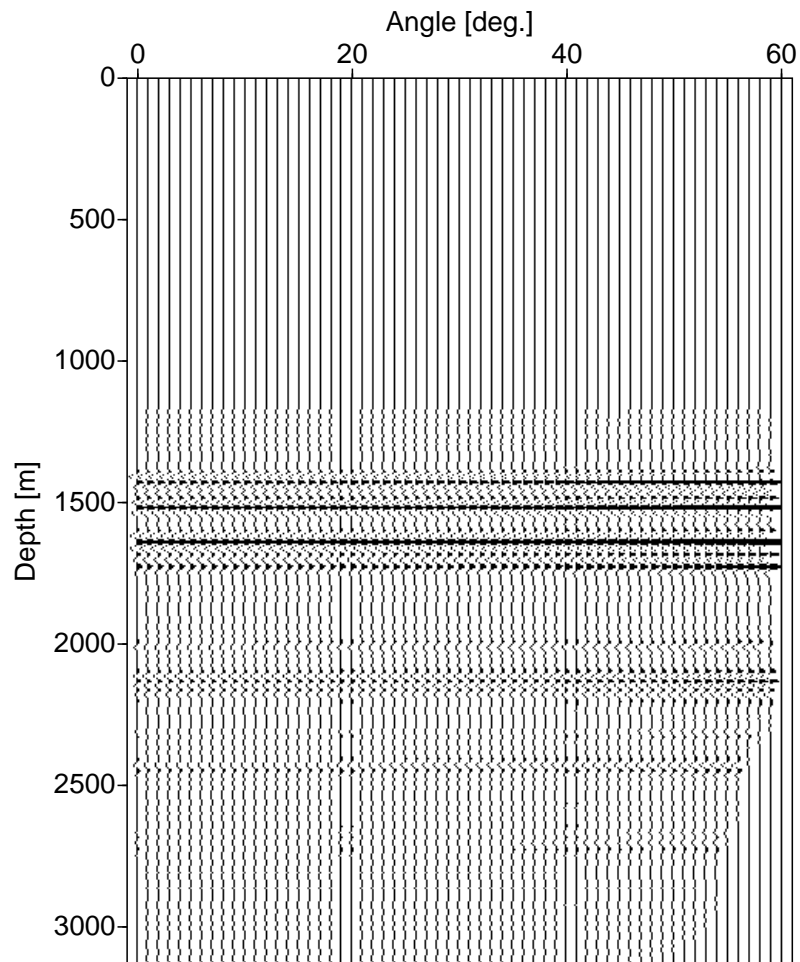


Figure 6.18: Common image gather at $CMP = 1069$ for real data.

Chapter 7

Conclusions

Today, the goal of migration has extended from imaging subsurface structures to recovering elastic properties. As the rock physical parameters are not related linearly to the seismic reflection data, usually, the inversion for elastic constants is performed by two linear sub-step: true amplitude pre-stack depth migration and, AVO/AVA analysis. Since pre-stack migration has great advantages at the time of imaging complex geological structures over other seismic processing schemes; integrating AVO and imaging together should lead to a new class of algorithms capable of imaging the Earth's interior and retrieving the physical properties.

In this thesis, I proposed a linearized inverse strategy to perform amplitude versus angle (AVA) imaging and rock physical properties inversion by applying the conjugate gradient method on a ray-based Kirchhoff migration/inversion scheme in the angle domain. The structural complexity is incorporated in the AVA/AVO estimation problem. Model space regularization terms are applied to enforce a desired solution. In our case, the first order model derivatives and the l_1 model norm are incorporated to enhance the spatial continuity of reflectors and gain vertical resolution at the same time.

To make the algorithm efficient, the Green's functions are calculated using kinematic ray tracing. Furthermore, combining with target oriented ray tracing, our method takes into account all relevant arrivals from all directions by shooting dense up-going rays from the image points. Since the conjugate gradient algorithm calls

the forward and adjoint operators once in each iteration, the Green's functions are calculated in advance and stored in memory. Although the high memory storage is required, the strategy is still efficient to avoid extra calculation for the Green's function in each iteration.

It is also important to point out that the rock physical properties are directly recovered from pre-stack seismic data. AVA/AVO analysis is obtained as a byproduct of pre-stack migration/inversion. As the CIGs are obtained using Zoeppritz equation (PP wave). The inverted rock physical properties will make all events in CIGs flat and free of noise.

As mentioned in the above Chapters, the transmission loss is not taken into account. The inverted result degrades for deep reflectors targets. As exploration targets are usually found at greater depth, future work will concentrate on enhancing the image of deeper interfaces.

This research project has provided a unifying link between AVO based interpretation and pre-stack imaging. The l_2 and l_1 norms are applied as regularization terms to enforce smoothness along the horizontal plane, and improve the vertical resolution as the same time. This is a new technique developed by our groups (Feng and Sacchi, 2004a). Since the inverted results not only depend on the data, but also rely on prior information, the inverted rock physical properties are more geologically consistent. A similar working strategy is also explored by Downton and Lines (2004). Hopefully, new developments in this area will be seen in the near future.

References

- Aki, K., and Richards, P. G., 1980, Quantitative Seismology: Theory and Methods: W. H. Freeman and Co.
- Alford, R., Kelly, K., and Boore, D., 1974, Accuracy of finite-difference modeling of the acoustic wave equation: *Geophysics*, **39**, 834–842.
- Beretta, M., Bernasconi, G., and Drufuca, G., 2002, Avo and ava inversion for fractured reservoir characterization: *Geophysics*, **67**, 300–306.
- Berkhout, A. J., and Wapenaar, C., 1993, A unified approach to acoustical reflection imaging: Part 2: The inverse problem: *J. Acoust. Soc. Am.*, **93**, 2017–2023.
- Berkhout, A., 1985, Seismic migration: Imaging of acoustic energy by wavefield extrapolation A Theoretical Aspects: Elsevier Science Publ.
- Berkhout, A. J., 1987, Applied seismic wave theory: Elsevier.
- Beydoun, W. B., and Mendes, M., 1989, Elastic ray-born l_2 -migration/inversion: *Geophys. J.*, **97**, 151–160.
- Beylkin, G., and Burridge, R., 1990, Linearized inverse scattering problems in acoustics and elasticity: *Wave Motion*, **12**, 15–52.
- Beylkin, G., 1985, Imaging of discontinuities in the inverse scattering problem by inversion of a causal generalized radon transform: *J. Math. Phys.*, **26**, 99–108.
- Bleistein, N., and Gray, S. H., 2002a, From the hagedoorn imaging technique to kirchhoff migration and inversion: Center for Wave Phenomena, Colorado School of Mines.
- 2002b, A proposal for common-opening-angle migration/inversion: Center for Wave Phenomena, Colorado School of Mines.
- Bleistein, N., Cohen, J. K., and Stockwell, J. W., 2001, Mathematics of multidimensional seismic imaging, migration, and inversion: Springer.
- Bleistein, N., 1986, Two-and-one-half dimensional in-plane wave propagation: *Geophysical Prospecting*, **34**, 686–703.
- Bleistein, N., 1987, On the imaging of reflectors in the earth: *Geophysics*, **52**, 931–942.

-
- Bortfeld, R., 1961, Approximation to the reflection coefficients of plane longitudinal and transverse waves: *Geophys. Prosp.*, **9**, 485–502.
- Burridge, R., De Hoop, M. V., Miller, D., and Spencer, C., 1998, Multi-parameter inversion in anisotropic media: *Geophys. J. Internat.*, **134**, 757–777.
- Cerveny, V., Molotkov, I., and Psencik, I., 1977, *Ray method in seismology*: University of Karlova Press.
- Claerbout, J. F., 1992, *Earth Soundings Analysis: Processing versus Inversion*: Blackwell Scientific Publications.
- de Bruin, C., Berkhout, A. J., and Wapenaar, C., 1990, Angle dependent reflectivity by means of prestack migration: *Geophysics*, **55**, 1223–1234.
- de Bruin, C., 1992, *Linear AVO inversion by prestack depth migration: Imaging angle dependent reflectivity as a tool for litho-stratigraphic inversion*: Ph.D. thesis, Delft University of Technology.
- de Hoop, M., Burridge, R., Spencer, C., and Miller, D., 1994, Generalized radon transform amplitude versus angle (GRT/AVA) migration/inversion in anisotropic media: *Proc. SPIE*, **2301**, 15–27.
- Dix, C., 1955, Seismic velocities from surface measurements: *Geophysics*, **20**, 68–86.
- Downton, E. J., and Lines, R. L., 2001, Constrained 3 parameter AVO inversion and uncertainty analysis: 2001 CSEG National Convention.
- Downton, E. J., and Lines, R. L., 2002, AVO NMO: 2002 CSEG National Convention.
- Downton, E. J., and Lines, R. L., 2003, High-resolution AVO NMO: 2003 CSEG National Convention.
- Downton, E. J., and Lines, R. L., 2004, Three term AVO waveform inversion: 2004 CSEG National Convention.
- Duquet, B., Marfurt, K., and Dellinger, J., 2000, Kirchhoff modeling, inversion for reflectivity, and subsurface illumination: *Geophysics*, **65**, 1195–1209.
- Fatti, J. L., Smith, G. C., Vail, P. J., Strauss, P. J., and Levitt, P. R., 1994, Detection of gas in sandstone sandstone reservoirs using avo analysis: a 3-d seismic case history using the geostack technique: *Geophysics*, **59**, 1362–1376.
- Feng, J., and Sacchi, M., 2004a, High Resolution Regularized Least Squares AVA Kirchhoff Migration: 74th Ann. Internat. Mtg., Soc. Expl. Geophys., Expanded Abstracts.
- 2004b, Rock properties inversion with Kirchhoff AVAmigration/inversion: 2004 CSEG National Convention.
- Gray, S. H., Etgen, J., Dellinger, J., and Whitmore, D., 2001, *Seismic migration problems and solutions*: Veritas DGC Inc.

-
- Gray, S. H., 1997, True-amplitude seismic migration: A comparison of three approaches: *Geophysics*, **62**, 929–936.
- Green, G., 1839, On the laws of reflexion and refraction of light: *Transactions of the Cambridge Philosophical Society*, **7**.
- Hertweck, T., 2000, Practical aspects of the unified approach to seismic imaging, MSc thesis: Karlsruhe University.
- Jin, S., Madariaga, R., Virieux, J., and Lambaré, G., 1992, Tow-dimensional asymptotic iterative elastic inversion: *Geophys. J. Int.*, **108**, 575–588.
- Knott, C., 1899, Reflection and refraction of elastic waves with seismological applications: *Philosophical Magazine*, **48**, 64–97.
- Koefoed, O., 1955, On the effect of Poisson's ratio of rock strata on the reflection coefficients of plane wave: *Geophys. Prosp.*, **3**, 381–387.
- Kravtsov, Y. A., and Orlov, Y. I., 1990, *Geometrical optics of inhomogeneous media*: Springer.
- Kuehl, H., and Sacchi, M., 2003, Least squares wave equation migration for AVP/AVA inversion: *Geophysics*, **68**, 262–273.
- Kuehl, H., 2002, Least-squares wave-equation migration/inversion, Ph.D. thesis: University of Alberta.
- LeBras, R., and Clayton, R., 1988, A iterative inversion of back-scattered acoustic waves: *Geophysics*, **53**, 501–508.
- Li, Y. Y., Goodway, B., and Downton, J., 2003, Recent advances in application of avo to carbonate reservoirs: *Recorder*, **28**, 34–40.
- Lines, L. R., Slawinski, R., and Bording, R. P., 1999, A recipe for stability of finite-difference wave-equation computations: *Geophysics*, **64**, 967–969.
- Lumley, D. E., and Beydoun, W. B., 1997, Elastic parameter estimation by kirchhoff prestack depth migration/inversion: *SEP report*, **70**, 162–190.
- Rüger, A., 2002, Reflection coefficients and azimuthal AVO analysis in anisotropic media: *Society of Exploration Geophysicists*.
- Sacchi, M. D., Moldoveanu-Constantinescu, C., and Feng, J., 2003, Enhancing resolution via non-quadratic regularization - next generation of imaging algorithms: *CSEG Convention*.
- Sacchi, M. D., 1997, Reweighting strategies in seismic deconvolution: *Geophys. J. Int.*, **129**, 651–656.
- Scale, J. A., and Smith, M., 1994, *Introductory geophysical inverse theory*: Samizdat press.
- Scale, J. A., 1987, Tomographic inversion via the conjugate gradient method: *Geophysics*, **52**, 179–185.
-

-
- Shuey, T., 1985, A simplification of the Zoeppritz equations: *Geophysics*, **50**, 609–614.
- Strang, G., 1986, *Introduction to Applied Mathematics*: Wellesley-Cambridge Press.
- Tarantola, A., 1984, Linearized inversion of seismic reflection data: *Geophys. Prosp.*, **32**, 998–1015.
- Tarantola, A., 1986, A strategy for nonlinear elastic inversion of seismic reflection data: *Geophysics*, **51**, 1893–1903.
- Tarantola, A., 1987, *Inverse problem theory: Methods for data fitting and model parameter estimation*: Elsevier Science Publishing Company Inc.
- Thierry, P., Operto, S., and Lambaré, G., 1999, Fast 2d ray+Born migration/inversion in complex media: *Geophysics*, **64**, 162–181.
- Vanelle, C., 2002, *Traveltime-based true-amplitude migration*, Ph.D. thesis: Hamburg University.
- Versteeg, R., and Grau, G., 1991, The Marmousi experience: Proceedings of the 1990 EAEG Workshop, 52 EAEG Meeting, Eur. Assoc. Expl. Geophys.
- Versteeg, R., 1994, The Marmousi experience: Velocity model determination on a synthetic complex data set: *The Leading Edge*, **13**, no. 09, 927–936.
- Wang, Y., 1999, Approximations to the Zoeppritz equations and their use in AVO analysis: *Geophysics*, **64**, 1920–1927.
- Wiggins, R., Kenny, G. S., and McClure, C., 1983, A method for determining and displaying the shear-velocity reflectivities of a geologic formation: European Patent Application 0113944.
- Xu, S., Chauris, H., Lambaré, G., and Noble, M., 2001, Common-angle migration: A strategy for imaging complex media: *Geophysics*, **66**, 1877–1894.
- Xu, Y., 2003, Angle-dependent amplitude and AVO/AVA analysis with PSDM: 2003 CSEG National Convention.
- Youzwishen, C., 2001, *Non-linear sparse and blocky constraints for seismic inverse problems*, MSc. thesis: University of Alberta.
- Zoeppritz, K., 1919, On the reflection and penetration of seismic wave through unstable layers: *Göttinger Nachrichten*, **1**, 66–84.